Journal of Hazardous Materials 430 (2022) 128383

Contents lists available at ScienceDirect

Journal of Hazardous Materials

journal homepage: www.elsevier.com/locate/jhazmat

Review

Monopersulfate in water treatment: Kinetics

F. Javier Rivas

Departamento de Ingeniería química y química física, IACYS,Universidad de Extremadura, Av. Elvas s/n, 06006 Badajoz, Spain

HIGHLIGHTS

- A detailed radical mechanism of peroxymonosulfate decomposition is applied.
- Some of the elemental reactions used can be neglected due to low/null influence.
- Use of pseudofirst order kinetics is an oversimplified strategy in most cases.
- Influence of main operating variables can be theoretically modelled.
- A generic model is proposed to simulate peroxymonosulfate based systems.

GRAPHICAL ABSTRACT

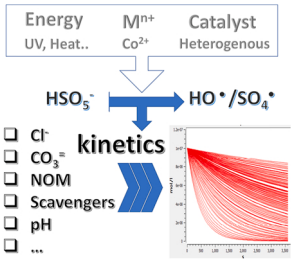

ARTICLE INFO

Editor: Yang Deng

Keywords:
Peroxymonosulfate
Kinetics modelling
Variables influence
Radical mechanism

ABSTRACT

The kinetics of monopersulfate based systems in the elimination of potential harmful contaminants has been assessed from a theoretical point of view. A detailed reaction mechanism sustained in the generation of radicals (mainly hydroxyl and sulfate), propagation and termination stages has been proposed. The system of first order differential equations derived has numerically been solved. The effect of main influencing parameters such as contaminant and peroxymonosulfate initial concentrations, intermediate generation, presence of organic matter, role played by anions, has been theoretically obtained. Discussion of simulated results has been accomplished by comparison with experimental data found in the literature. At the sight of the theoretical and empirical data, use of simplistic pseudo first order kinetics is discouraged. Despite considering a significant number of elemental reactions, modelling of the system reveals that a high fraction of them can be neglected due to their insignificant role played in the mechanism. The entire mechanism has been tested when peroxymonosulfate has been activated by UV radiation, although results can be fairly extrapolated to other activation strategies. Finally, a generic model capable of accounting for the effect of a diversity of parameters is proposed. No theoretical background is behind the model, however the generic model clearly improves the results obtained by simple first order kinetics.

1. Introduction

According to United Nations (United Nations: Sustainable development goals, 2021), water shortage affects more than 40 per cent of Earth population and, what is of major concern, this scarcity is expected to rise in the near future. More than 1.7 billion people are currently living in river basins where water use exceeds natural or artificial recharge. Under this distressing scenario, more than 80 per cent of wastewater from anthropogenic origin is discharged into rivers or sea without any contamination reduction.

Amongst the targets proposed by United Nations, by 2030 society must improve water quality through water pollution reduction. Two principal alternatives are considered, the most desirable is minimization of contaminants release. The other way is effective and sustainable application of pollution removal technologies. The goal to be achieved is halving the amount of untreated wastewater simultaneously increasing recycling and safe reuse (United Nations: Sustainable development goals, 2021). In any case, the costs of adequate wastewater management are significantly outweighed by the benefits to human health, economic development, and environmental sustainability (United Nations: Water

https://doi.org/10.1016/j.jhazmat.2022.128383
Received 29 October 2021; Received in revised form 22 December 2021; Accepted 26 January 2022
Available online 31 January 2022

Policy Brief: Water Quality, 2011).

Water treatment can be approached through different alternatives depending on the perspectives for final use/recycling, contamination nature and pollution load. As a rule of thumb, when suitable, biological processes is the preferred option in wastewater treatment systems and micropollutants abatement. Simplicity and attractive economy aspects are under this preferential usage. Biological based treatments go back to early years of the 20th century. The activated sludge methodology was first reported in 1913 (Henze et al., 2008).

However, in some circumstances, biological processes are not adequate and bio recalcitrant/toxic compounds cannot be treated in conventional wastewater plants (Merle et al., 2009; Sarria et al., 2002; Santiago et al., 2004). Different approaches are considered including physicochemical processes such as precipitation flocculation (Jørgensen, 1979; Guerreiro et al., 2020; Lal and Garg, 2017; Pantziaros et al., 2018) membrane filtration (Ayol et al., 2021; Hongchao Li et al., 2021; N. Li et al., 2021; Y. Li et al., 2021; Nesan et al., 2021; Saravanan et al., 2021), adsorption (Cheng et al., 2021; Oba et al., 2021; Sivaranjanee and Kumar, 2021) or/and chemical oxidation/reduction (Chauhan et al., 2021; Divyapriya et al., 2021; Javaid et al., 2021). Amongst oxidation technologies, advanced oxidation processes (AOPs) are widely studied as an efficient alternative and promising option in the next future. (Ma et al., 2021). These processes are based on the generation of powerful free radicals (mainly $HO^{\bullet}$) capable of unselectively attack a significant number of organic and inorganic compounds. The future of AOPs relies on reducing the high energy demand and elevated costs associated to their application (Miklos et al., 2018). Research on AOPs implementation has been focused both in individual compounds and complex wastewater matrix (Antonopoulou et al., 2021; Ashraf et al., 2021; Bhat and Gogate, 2021; Davididou and Frontistis, 2021; Dinh et al., 2020; Domingues et al., 2021; Giannakis et al., 2021; Korpe and Rao, 2021; Hongchao Li et al., 2021; Y. Li et al., 2021; N. Li et al., 2021; Mpatani et al., 2021). Broadly speaking, works based on the application of AOPs focus on assessing the efficiency in contamination removal, influence of different parameters, catalyst characterization and, to a lesser extent, kinetic analysis of the process. This is particularly evident in sulfate radical based processes, likely due to the more recent appearance of this technology in the field of water and wastewater treatment.

Modelling of process kinetics is the base of reactor and plant treatment design (Berger et al., 2001; Zalazar et al., 2004). At this point, a dilemma emerges when facing complicated systems, (as it is the case of AOPs). Advanced oxidation processes proceed through the development of a huge number of elemental reactions, in series and parallel, involving initiation, chain propagation and termination stages. In some cases, a number of these stages is difficult to evaluate/identify. Hence, the generation, existence or role played by some species is not always warranted or conveniently proven. The role played by generated organic radicals (i.e. organic peroxyradicals), the importance of inorganic radicals generated from carbonates, chlorides, nitrates, etc., the presence of initiators or chelating agents, the development of useless side reactions such as peroxide decomposition, etc. are not well assessed (Rivas et al., 2003, 2002, 1998). Moreover, some of the aforementioned issues affect the process to a different extent, depending on the operating conditions and water matrix nature. Additionally, identification and quantification of intermediates with time is practically impossible, so the influence of the presence of these intermediates cannot be adequately evaluated or considered rigorously.

Consequently, modelling of AOPs processes can be faced from two different points of view. On one hand, the ultimate task of a kinetic expression/model can be assumed to simulate the process around the operation point with the hope that conditions are not going to significantly change. In this case, there is no need to handle complicated mathematical expressions or reaction mechanisms. Simple models such as pseudo first order kinetics are then applied (Liu et al., 2020; Pérez-Moya et al., 2011; Wu et al., 2019; Meng et al., 2020). On the other hand, the alternative is to consider a set of elemental reactions involving radicals, molecular reactions, mass transfer processes, radiation models, equilibriums, etc. Obviously, all the above lead to formulation of complicated models in differential equations form that must be solved (Djaballah et al., 2021; Ko et al., 2009; T. Zhang et al., 2019; Z. Zhang et al., 2019; Zhou et al., 2018). A third option could be a mixture of the previous strategies, i.e., use of elemental reactions and simplified expressions to simulate, for example, radiation distribution in the photoreactor, or applying the hypothesis of steady state to radicals (Solís et al., 2019).

Both kinetic approaches present some advantages and disadvantages. Hence, use of simplistic first order kinetics involves not only the easiness of mathematics but a rapid method to compare different technologies (from a kinetic point of view). Also, first order kinetics is the starting point to calculate some figure of merits related to the economy of the specific process applied (Bolton et al., 2001). Drawbacks arise from the lack of a solid kinetic base behind. In most of cases, experiments carried out at different initial concentration of the target compound reveal a significant dependency of the observed rate constant with parent compound concentration at time zero, discarding therefore, the development of pure pseudofirst order kinetics. This error is frequently found in the specialized literature, so data obtained is of limited (if any) value. Pseudo first order kinetics application becomes just a fitting process which, in some cases even results in a poor fitting process.

Use of a detailed reaction mechanism involves the knowledge of elemental reactions. These elemental reactions should sustain the influence of operating variables, determine the evolution of radical species, predict the influence of scavenging substances, etc. Difficulties arise when considering reaction intermediates, formation of complexes that change initiation rate stages, inefficient decomposition of peroxides, etc. Application of detailed reaction mechanisms is the preferred option from an academic point of view. Likely, simplified models are the desired alternative for water treatment practitioners.

A brief compilation of recent works focused on the use of peroxymonosulfate as radical promoter in water and wastewater treatment (see Table 1) reveals that a significant percentage of them sustains the kinetic conclusions in the application of simplistic pseudo first order expressions. Moreover, frequently, experiments carried out at different initial concentrations of target compounds uncover that k_{obs} (the pseudofirst order rate constant) depends on the initial load of the parent compound. This behavior is inconsistent with pure pseudo first order kinetics. In any case, detailed reaction mechanisms, despite of being a more useful tool than simplistic expressions, are not normally capable of adequately modelling the process under all possible scenarios. Likely, a consensus between both strategies should be adopted. The proposal of pseudoempirical models, simulating the influence of main variables around the operation point, seems to be the best choice.

The objective of this work is the resolution of a detailed mechanism involving the highest number of elemental reactions derived from the use of monopersulfate in water. The system of first order differential equations was solved by using a complex pathway simulator (Hoops et al., 2006). Use of a generic compound would eventually allow the identification of key stages and secondary reactions that could be neglected. In general, the related bibliography does not elucidate the key and non-influencing steps from a quantitative point of view. Theoretical results obtained are also the base to discard simple pseudo first order expressions, commonly applied in the literature (see Table 1). The effect of operating variables is analyzed and compared to results reported in previous works. An in-depth discussion is accomplished to consider the different and, in some cases opposite, influence of the same variable found in some investigations.

As stated previously, use of a pseudo-empirical model is an option of compromise between the complexity of a detailed reaction mechanism and the simplicity of a logarithmic fitting process. Accordingly, an attempt has been made to achieve an intermediate model capable of

Table 1
Brief summary of PMS based technologies for contaminant abatement.

Activation method	Target compound	Experimental conditions	Notes	Reference
CO_3^{2-}/PMS	Bisphenol A	BPA = 0.05 mM, CO_3^{2-} = 5 mM, and PMS = 1 mM	0.006–0.09 min^{-1} rate constants. Initial BPA effect discards pseudofirst order kinetics	(Abdul et al., 2021)
Co(II)/PMS	Chloramphenicol	[Co2 +]0 = 0.01 mM, [PMS]0 = 4 mM, no pH adjustment.	0.006–0.1 min^{-1} rate constants. Initial target compound effect discards pseudofirst order kinetics	(Xue et al., 2021)
HPO_3^{2-} /PMS	Several contaminants	[pollutants] = 20 mg/L, [PMS] = 10.0 mM, [HPO_3^{2-}] = 25.0 mM, pH = 7.06.	Psudofirst order kinetics applied. Study of inorganic anions influence. 0.02–0.15 min^{-1} rate constants.	(J. Peng et al., 2021; Y. Peng et al., 2021; G. Peng et al., 2021)
PMS/Cyclam Mn(II)	RBR K-2BP	MnL = 1.0–10 μM. $[substrate]_0$ = 20 mg/L PMS = 0.1–1.0 mM. pH= 3.0–11.0. T = 15–30 °C)	Psudofirst order kinetics applied at different operating conditions. Rate constants varies with parameter values	(Yu et al., 2020)
Fe/Fe3O4/PMS	Iopamidol, atrazine	[IPM] = [ATZ] = 5.0 mg L− 1, [PMS] = 25.0 mg L− 1, Fe/Fe3O4 dose = 0.5 g L− 1	Pseudo first order kinetics with rate constants as high as 1.5 min^{-1}.	(Hu et al., 2021)
Tourmaline/ Perovskite/ PMS	Methylene blue	T = 25 ℃, [PMS] = 0.2 g/L, [catalyst] = 0.1 g/L, pH = 7.8	0.66 − 0.26 min^{-1}. MB influence discards first order kinetics	(Wang et al., 2021)
Cu0.76Co2.24O4/SBA-15/PMS	Sulfapyridine	[catalyst]= 1.0 g/L, [SPD]= 50 μmol/L, [PMS]/[SPD]= 20, [pH]= 7.	0.03–0.06 min^{-1} rate constants. Initial sulfapyridine influence discards first order kinetics	(He et al., 2021)
$Co_{1+x}Fe_{2-x}O_4$/PMS	Rhodamine B	$[RhB]_0$ = 40 mg/L, [catalyst] = 200 mg/L, [PMS] = 200 mg/L pH_0 = 5, T = 25 °C	Pseudofirst order in the order = 0.26 min^{-1}. No runs at different RhB concentration completed	(Zhao et al., 2021)
FeS@biochar / PMS	2,4-dichlorophenoxyacetic (2,4-D)	[catalyst] = 500 mg/L, [PMS] = 0.65 mM, [2,4-D] = 0.045 mM, pH_0 = 3.4.	Langmuir type kinetics with zero or first order depending on limiting stage	(Hong et al., 2021)
Goethite/biochar/PMS	Tetracycline (TC)	[catalyst] = 50 mg/L, [PMS] = 1 mM, [TC] = 30 mg/L and T = 298 K.	0.013–0.021 min^{-1} rate constants with special relevance of singlet oxygen. Initial TC effect discards used kinetics	(C. Guo et al., 2021; Y. Guo et al., 2021)
CuCo-MOF-74/PMS	Methylene blue (MB)	PMS = 2.0 mM; MB = 0.2 mM; catalysts = 100 mg/L; T = 25 °C.	Pseudofirst order rate constant in the range 0.02–0.18 min^{-1}. Experiments at different MB initial concentration discard first order kinetics	(Li et al., 2021a)
Fe2Mn1-Fe@NC/PMS	4-aminobenzoic acid ethyl ester (ABEE)	20 mg/L ABEE solution, 0.1 g/L catalyst and 0.1 mM PMS	Maximum rate constant 0.4238 min^{-1}	(Y. Huang et al., 2021; Z. Huang et al., 2021)
CuM@Fe_3O_4 (M= Mg, Zn, Ca, Ba, Al)/PMS	Acetaminophen (ACE)	[ACE] = 0.03 g/L, [PMS] = 0.153 g/L, [catalysts] = 0.05 g L− 1, $[pH]_0$ = 7, T = 30 °C.	Important role played by $^1O_2$Pseudofirst order rate constant in the range 0.002–0.242 min^{-1}	(Zhou et al., 2021)
Carbonized polyaniline/PMS	Phenol	[Phenol] = 10 μM, [Catalyst] = 25 mg/L, [PMS] = 0.5 mM, initial pH = 7.0.	Pseudofirst order rate constant in the range 0.011–0.373 min^{-1}	(Liu et al., 2021)
Cu in $LaMnO_3$ / PMS	Sulfomethoxazole	20 mg catalyst in 100 mL sulfomethoxazole solution 19.8 μmol/L and PMS (1.3 mmol/L).	First order kinetics in the range 0.02 – 0.2 min^{-1}	(Gao et al., 2021)
Fe3C@CN_CF/PMS	Bisphenol A	V = 30 mLFe3C@CN/CF= 0.2 g/ LBPA = 20 mg/L PMS = 9.0 mg	Application of first order kinetics. Concentration profiles suggest kinetics other than first order. Rate constant 0.089 min^{-1}	(Y. Guo et al., 2021; C. Guo et al., 2021)
Co/CNTs/PMS	Metylparaben	[MeP] = 10 μM, [PMS] = 40 μM, [Co/CNTs] = 2 mg/L, pH 7.0, 25 °C	Study of the influence of anions (Cl-). Use of first order kinetics	(G. Peng et al., 2021; Y. Peng et al., 2021; J. Peng et al., 2021)
Ag/ZnO/ PMS/Vis	p-nitrophenol	[photocatalyst] = 0.5 g/L; [p-NP] = 30 mg/LPMS = 0.1–5 mM.	Use of first order kinetics applied at different temperatures and PMS doses	(Truong et al., 2021)
Fe1Co1-MOF-74/PMS	phenanthrene	PMS = 0.2 mM; phenanthrene = 1.0 mg/L; catalysts = 50 mg/L; initial pH = 3.15; T = 25 °C	First order rate constants in the order of 0.1 min^{-1}	(Li et al., 2021b)
(CeO2)/ US/PMS	tetracycline	temperature: 25 ± 1 °C; 0.6 g/L catalyst, C = 15 mg/L, 50 mM oxidant, 50 W US power	Zero order kinetics were applied	(Asadzadeh et al., 2021)
Ni_2P/PMS	Dyes, MB	[MB], 100 mg L^{-1}; [Ni2P], 150 mg L^{-1}; [PMS], 150 mg L^{-1}; temperature, 30 °C	Pseudofirst order rate constants depend on MB concentration (06–0.08 min^{-1}).	(Wan et al., 2020)
UV/O_3/PMS	Atenolol	[O_3] = 2.6 mg/L min− 1, [PMS]0 = 66.4 mg/L, pH = 6.0.	0.3–0.9 min^{-1} rate constants. Initial target compound effect discards pseudofirst order kinetics although final conversion is similar, A model based on steady state concentration is applied	(Yu et al., 2021c)
UV_254 / PMS	Tris(2-chloroethyl) phosphate	PMS = 5–75 mg/L TCEP = 1 mg/LT= 26 ± 1 °C pH 6.6–7.0	Application of first order kinetics with rate constant in the range 0.03–0.15 min^{-1}, depending on conditions under 5 mW cm^{-2} of irradiation. Influence of TCEP initial concentration discards first order kinetics.	(Yu et al., 2021a)
UV_254 / PMS	tris-(2-chloroisopropyl) phosphate	Temperature 24 ± 2 °C, pH 6.7–7.0, PMS 100 mg L− 1, TCPP 1 mg L− 1	Application of first order kinetics with rate constant in the range 0.01–0.4 min^{-1}	(Yu et al., 2021b)
UV_254 / PMS	Diclofenac	DCF] = 1 μM, [PMS] = 50 μM	Experiments at different initial concentration of diclofenac discard pseudofirst order kinetics	(G. Peng et al., 2021; J. Peng et al., 2021; Y. Peng et al., 2021)
Solar / PMS				(Solís et al., 2020)

(*continued on next page*)

Table 1 (*continued*)

Activation method	Target compound	Experimental conditions	Notes	Reference
	Pharmaceuticals and personal care products	T = 293 K, PMS, = 0.5 mM, V = 500 mLPPCP 0.1–1.0 ppm	Pseudoempirical reaction mechanism based on elemental reactions. Some rate constants as a function of operating parameters	
VUV/UV/PMS	Bisphenol A	[BPA] = 0.022 mM, pH = 7, T = 20 °C	Mechanism based on radical steady state conditions. Initial BPA concentration influences pseudofirst order rate constants	(Lin et al., 2020)
UVA Leds/PMS	Pharmaceuticals	Ph = 100 μg L^{-1}; pH = 7.6; [PMS] = 0.1 mM.	Pseudofirst order k_{Obs} reported for individual compounds in the range 0.15–0.1 min^{-1}	(Guerra-Rodríguez et al., 2021)
UV_254/ PMS	Chloral hydrate	[CH]o = 10 μM, [pH]o = 7.0, T = 23 °C, [PMS]o = 50–200 μM	Pseudofirst order rate constants in the order 0.1–0.5 min-1	(Zhang et al., 2021)
UV_254/ PMS	Methotrexate	[MTX]o = 5 mg·L^{-1}, PMS = 1–4 mM, pH = 3.3	Pseudofirst order rate constant in the range 0.03–0.15 min-1 dependent on initial MTX concentration	(Kanjal et al., 2020)

taking into consideration the effect of the most influencing parameters without introducing poorly manageable differential equations.

2. Results and discussion

The kinetics of PMS activated systems will be first handled by accounting for the elemental stages proposed in the literature. The effect of different variables and influencing parameters will be theoretically simulated and discussed.

2.1. Homogeneous initiation reactions

Activation of PMS can be accomplished through different pathways. For instance in the presence of radiation (Berruti et al., 2021), by homogeneous or heterogeneous catalysts (Hou et al., 2021), heat or even ultrasounds (Rivas et al., 2008), more examples can be found elsewhere (Wang and Wang, 2018).

Likely, catalytic homogeneous or energy-based activation is the simplest process in terms of modelling. The presence of a solid phase and mass transfer limitations are avoided compared to heterogeneous catalytic systems. In homogeneous catalysis, difficulties arise from the fact that normally, the catalyst used is a transition metal involving a redox cycle. The high probability of complexation of the catalyst makes difficult to know/determine both the initiating reaction to generate radicals and/or the reduction reaction to complete the redox cycle. Hence, Gimeno et al. (2009) made an attempt to model the system PMS/Co(II) in ultrapure water assuming an initiation reaction rate between PMS and Co(II) similar to the one reported in the Fenton chemistry between hydrogen peroxide and Fe(II). Values of comparable order are reported in the reaction of peroxides and transition metals in ultrapure water. Hence, a value of 27 $M^{-1}s^{-1}$ has been reported for the reaction between persulfate and Fe(II) (Ike et al., 2018). Given the insolubility of Co(III), the existence of a reduction stage from Co(III) to Co(II) through the reaction with PMS seems to be a crucial stage in the continuity of the system efficiency (Zhang and Edwards, 1992):

$$HSO_5^- + Co(II) \rightarrow OH^- + Co(III) + SO_4^{-\bullet} \quad (1)$$

$$HSO_5^- + Co(II) \rightarrow Co(III) + HO^\bullet + SO_4^{2-} \quad (2)$$

$$HSO_5^- + Co(III) \rightarrow Co(II) + H^+ + SO_5^{-\bullet} \quad (3)$$

Based on the previous work, variation of the reaction rate of Eq. (3) was suggested depending on the complexing capacity of substances present in the system (Rivas et al., 2012). Besides reactions 1 and 2, some authors have claimed the formation of a Co(II)-PMS complex as the primary reactive species instead of free radicals. This complex would have the ability to conduct both one-electron-transfer and oxygen-atom-transfer reactions at different rates depending on pH (N. Li et al., 2021; Y. Li et al., 2021; Hongchao Li et al., 2021). In any case, regardless of the species involved in the oxidation process, the kinetics should not be affected provided that the rate constant between the complex and the target compound is adequately fitted/determined. Other homogeneous metallic catalysts have also been suggested to be adequate in PMS activation (Anipsitakis and Dionysiou, 2004), although Co(II) seems to be the preferred activator.

In the case of high valence iron cations (mainly ferrate, Fe(VI)), the oxidation capacity of the system PMS/Fe(VI) has recently been attributed to a pathway via two electron transfer to generate the ferryl ion, Fe (IV), which is a stronger oxidant than Fe(VI). Fe(IV) presents a similar reactivity than the perferryl ion, Fe(V), generated after reduction of Fe (VI) with $Fe(OH)_2$ (Luo et al., 2021). High valence iron cations are more selective than radicals and their oxidation capacity is highly dependent on target compound structure. Contrarily, other authors maintain the relevant role played by sulfate and hydroxyl radicals when combining ferrate and PMS (Gong et al., 2020; Wu et al., 2018). PMS can also be activated by Fe(II) (Guyu and Kee, 2022; Wang et al., 2022), again the nature of generated oxidant species is a matter of controversy and some authors claim the coexistence of both, radical and ferryl species (Dong et al., 2021; Milh et al., 2022). The kinetics of this type of processes should be specifically studied to discern the main oxidant species generated, their reactivity with target compounds and the limiting stages to be considered.

Another PMS activation pathway is the use of radiation. Apparently, PMS photolysis should lead to formation of radicals according to (Qi et al., 2019; Guan et al., 2011):

$$HOOSO_3^- \xrightarrow{h\nu} HO^\bullet + SO_4^{-\bullet} \quad (4)$$

In order to avoid complex equations to model radiation incidence inside the reactor, or facing the use of the local volumetric rate of photon absorption (if heterogeneous photocatalysts are used), a simplistic Lambert Beer expression can be applied when no photocatalysts are present:

$$-\frac{dC_{PMS}}{dt} = \varphi_{PMS} I_o \frac{\varepsilon_{PMS} C_{PMS}}{Absorbance}[1 - \exp(-2.303 \times L \times Absorbance)] \quad (5)$$

where φ_{PMS} is the quantum yield in the photolysis of PMS, I_o is the volumetric incident light intensity at 254 nm (Einstein L^{-1} s^{-1}), Absorbance is the radiation absorbed by the bulk solution, ε_{PMS} is the molar extinction coefficient of PMS, L is the optical path length for the reaction reactor (cm) and C_{PMS} is the concentration of peroxymonosulfate.

Generation of radicals through Eq. (4) necessitates the application of radiation of sufficient energy at low wavelength. Hence, the molar extinction coefficient of PMS at 254 nm is in the interval 14–150 $M^{-1}cm^{-1}$ (from pH 7–12), steadily decreasing to values close to zero as radiation wavelength increases (Ao and Liu, 2017; Guan et al., 2011). However, some authors have observed a synergistic effect of the combination PMS/UVA or PMS/Sunlight. PMS hardly absorbs light above 300 nm suggesting that above this wavelength, homolytic scission of the O-O bond is unlikely to occur (Berruti et al., 2021). However, at the same time, a negative effect has been experienced by the presence of

well-known radical scavengers (Solís et al., 2019). Photosensitization of organics present in the media could be a plausible explanation, as it is the case of clofibric acid (Solís et al., 2020), the role played by $^1O_2$ should also be considered, although this aspect remains unclear (Lee et al., 2020).

If the homogeneous activation of PMS is considered (either by Co(II) or 254 nm UV radiation), together with reactions 1–4 the following set of reactions could take place in the oxidation of a generic probe compound RH (Travina et al., 2006; Guan et al., 2011; Lutze et al., 2015; Hu and Long, 2016; Herrmann et al., 2000):

Propagation:

$$SO_4^{-\bullet} + HSO_5^- \rightarrow HSO_4^- + SO_5^{-\bullet}\ k < 1\times10^5\ M^{-1}s^{-1} \quad (6)$$

$$HO^\bullet + HSO_5^- \rightarrow SO_5^{-\bullet} + H_2O\ k = 1{\cdot}7\times10^7\ M^{-1}s^{-1} \quad (7)$$

$$HO^\bullet + SO_5^{2-} \rightarrow SO_5^{-\bullet} + OH^-\ k = 2{\cdot}1\times10^9\ M^{-1}s^{-1} \quad (8)$$

$$HO^\bullet + H_2O_2 \rightarrow HO_2^\bullet + H_2O\ \ k = 2.7\times10^7 M^{-1}s^{-1} \quad (9)$$

$$HO^\bullet + HO_2^- \rightarrow HO_2^\bullet + OH^-\ \ k = 7.5\times10^9 M^{-1}s^{-1} \quad (10)$$

$$HO_2^\bullet + H_2O_2 \rightarrow HO^\bullet + O_2 + H_2O\ \ k = 3.0 M^{-1}s^{-1} \quad (11)$$

$$O_2^{-\bullet} + H_2O \rightarrow HO^\bullet + O_2 + OH^-\ \ k = 0.13 M^{-1}s^{-1} \quad (12)$$

$$SO_4^{-\bullet} + H_2O \rightleftarrows OH^\bullet + HSO_4^-\ \ k = 6.6\times10^2 s^{-1} k- = 6.9\times10^5 M^{-1}s^{-1} \quad (13)$$

$$SO_4^{-\bullet} + OH^- \rightarrow OH^\bullet + SO_4^{2-}\ \ k = 6.5\times10^7 M^{-1}s^{-1} \quad (14)$$

$$2SO_5^{-\bullet} \rightarrow 2SO_4^{-\bullet} + O_2\ \ k = 2.15\times10^8 M^{-1}s^{-1} \quad (15)$$

Termination:

$$2SO_4^{-\bullet} \rightarrow S_2O_8^{2-}\ \ k = 7.5\times10^8 - 3.6\times10^9 M^{-1}s^{-1} \quad (16)$$

$$2SO_5^{-\bullet} \rightarrow S_2O_8^{2-} + O_2\ \ k = 3.5\times10^8 M^{-1}s^{-1} \quad (17)$$

$$2HO^\bullet \rightarrow H_2O_2\ k = 5{\cdot}2\times10^9\ M^{-1}s^{-1} \quad (18)$$

$$SO_4^{-\bullet} + HO^\bullet \rightarrow HSO_5^-\ k = 1.0\times10^{10} M^{-1}s^{-1} \quad (19)$$

$$SO_4^{-\bullet} + S_2O_8^{2-} \rightarrow S_2O_8^{-\bullet} + SO_4^-\ \ k = 6.5\times10^5 M^{-1}s^{-1} \quad (20)$$

$$HO^\bullet + S_2O_8^{2-} \rightarrow S_2O_8^{-\bullet} + OH^-\ \ k = 1.4\times10^7 M^{-1}s^{-1} \quad (21)$$

$$HO_2^\bullet + HO_2^\bullet \rightarrow O_2 + H_2O_2\ \ k = 8.3\times10^5 M^{-1}s^{-1} \quad (22)$$

$$HO_2^\bullet + O_2^{-\bullet} \rightarrow O_2 + HO_2^-\ \ k = 9.7\times10^7 M^{-1}s^{-1} \quad (23)$$

$$HO^\bullet + HO_2^\bullet \rightarrow H_2O + O_2\ \ k = 6.6\times10^9 M^{-1}s^{-1} \quad (24)$$

$$HO^\bullet + O_2^{-\bullet} \rightarrow OH^-\ + O_2\ \ k = 7.0\times10^9 M^{-1}s^{-1} \quad (25)$$

$$SO_4^{-\bullet} + Co(II) \rightarrow SO_4^{2-} + Co(III)\ k = 2{\cdot}0\times10^6\ M^{-1}s^{-1} \quad (26)$$

$$HO^\bullet + Co(II) \rightarrow HO^- + Co(III)\ k = 2{\cdot}0\times10^6\ M^{-1}s^{-1} \quad (27)$$

Additional reactions:

$$S_2O_8^{2-} + H_2O \rightarrow HSO_5^- + HSO_4^-\ \ k = 7.5\times10^{-5} M^{-1}s^{-1} \quad (28)$$

$$HSO_5^- \rightleftarrows H^+ + SO_5^{2-}\ \ pK_{eq} = 9.4 \quad (29)$$

$$H_2O \rightleftarrows H^+ + OH^-\ pK_{eq} = 14 \quad (30)$$

$$HSO_4^- \rightarrow H^+ + SO_4^{2-}\ \ k = 0.012 s^{-1} \quad (31)$$

$$H_2O_2 \rightleftarrows H^+ + HO_2^-\ \ pK_{eq} = 11.6 \quad (32)$$

$$HO_2^\bullet \rightleftarrows H^+ + O_2^{-\bullet}\ \ k = 3.2\times10^5, k- = 2.0\times10^{10} \quad (33)$$

$$H_2O_2 \longrightarrow^{h\upsilon} 2HO^\bullet \quad (34)$$

$$S_2O_8^{2-} \longrightarrow^{h\upsilon} 2SO_4^{-\bullet} \quad (35)$$

$$RH + SO_4^{-\bullet} \rightarrow Intermediate + SO_4^{2-}\ k = 10^9\text{-}10^{10}\ M^{-1}s^{-1} \quad (36)$$

$$RH + HO^\bullet \rightarrow Intermediate + HO^-\ k = 10^9\text{-}10^{10}\ M^{-1}s^{-1} \quad (37)$$

$$RH + HSO_5^- \rightarrow Intermediate\ k = f(RH)\ M^{-1}s^{-1} \quad (38)$$

$$Intermediate + SO_4^{-\bullet} \rightarrow Product + HSO_4^{2-}\ k = 10^9\text{-}10^{10}\ M^{-1}s^{-1} \quad (39)$$

$$Intermediate + HO^\bullet \rightarrow Product + HO^-\ k = 10^9\text{-}10^{10}\ M^{-1}s^{-1} \quad (40)$$

The proposed mechanism is based on the most simplistic situation where only one intermediate competes in oxidative reactions (with similar reactivity than RH), no organic radicals are generated, no matrix effects are considered, no photosensitization processes occur, and radicals apart of hydroxyl and sulfate do not attack the target compound RH. Also, other possible removal pathways such as direct photolysis or direct attack by peroxymonosulfate (Eq. 38) and the role played by $^1O_2$ are ruled out. Even taking into account the simplest scenario, the number of reactions is significant. However, although one can consider that the higher the number of reactions, the better the model, this is not completely true, and some stages can be ruled out because of their low extension. Hence, with the premise of elucidating the real important reactions, the previous mechanism can be solved for a generic case. The radical mechanism was tested by considering PMS activation by 254nm UV radiation at pH 7, using the molar extinction coefficients of PMS, persulfate and H_2O_2 as 14., 21 and 19 M^{-1} cm^{-1}, respectively. The quantum yield of radical generation by peroxides scission is taken as unity for the three initiators (Guan et al., 2011). The rest of operating parameters are absorbance = 0.01 (constant throughout the reaction), $C_{PMSo} = 1\times10^{-4}$ M, $C_{RHo} = 1\times10^{-7}$ M, $I_o = 1\times10^{-8}$ Einstein L^{-1} s^{-1} and L = 3 cm. Under the aforementioned conditions, the radical profiles

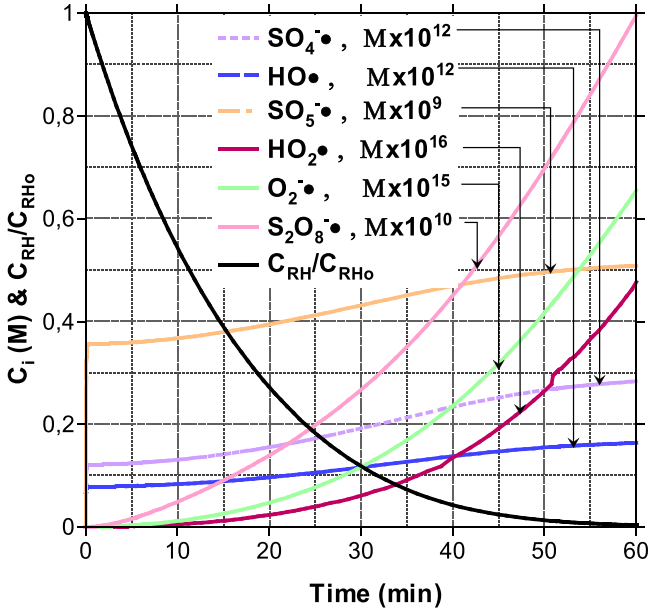

Fig. 1. Simulated removal of the generic compound RH by PMS activation under UV-C radiation. Evolution of RH and radicals concentration with time. Conditions: $C_{PMSo} = 1\times10^{-4}$ M, $C_{RHo} = 1\times10^{-7}$ M, $I_o = 1\times10^{-8}$ Einstein L^{-1} s^{-1}, L = 3 cm, pH = 7, T = 20 ºC.

shown in Fig. 1 were obtained. The proposed mechanism reveals the prevalence of sulfate and hydroxyl radicals over peroxy and hydroperoxyl radicals. Additionally, relative high concentrations of $SO_5^{-\bullet}$ and $S_2O_8^{-\bullet}$ suggest that scavenging of radicals by excess of PMS occurs to a significant extent (reactions 6–8). Recombination of $SO_5^{-\bullet}$ and $SO_4^{-\bullet}$ generates $S_2O_8^{2-}$ (accumulation after 60 min is 2×10^{-8} M compared to 3×10^{-13} M of H_2O_2) which further scavenges active radicals (Eqs. 20, 21) to form $S_2O_8^{-\bullet}$. The proposed mechanism does not consider that $SO_5^{-\bullet}$, $S_2O_8^{-\bullet}$, $HO_2^{\bullet}$ and $O_2^{-\bullet}$ are able to contribute to oxidative reactions, however, depending on the nature of the organics present in solution or intermediates formed, these organics can also be further degraded (Neta et al., 1988). Also, these radicals might react with some metals present in the media regenerating PMS (Rastogi et al., 2009; Travina et al., 2006).

A sensitivity analysis of the rate constant used in the mechanism revealed that not all the reactions considered influenced the removal rate of the generic parent compound RH. Hence, theoretically, reactions involving hydrogen peroxide and related radicals ($HO_2^{\bullet}$ and $O_2^{-\bullet}$) do not play an important role in the mechanism under the operating conditions used (reactions 9–12, 18, 22–25, 33 and 34). Also, sulfate-hydroxyl radical recombination (Eq. 19), radical scavenging by peroxydisulfate (Eqs. 20 and 21) and peroxydisulfate disproportionation (Eq. 28) do not seem to be important in PMS activated systems.

Key stages are, as expected, the photolysis rate of PMS, hydroxyl scavenging by PMS (Eqs. 7 and 8), the equilibrium between hydroxyl and sulfate radicals (Eq. 13) and formation of sulfate radicals from peroxymonosulfate radicals (Eq. 15). To a lesser extent, other influencing reactions under the conditions applied, are sulfate radicals scavenging by PMS (Eq. 6), transformation of sulfate radicals to hydroxyl radicals in alkaline conditions (Eq. 14) and formation of peroxydisulfate (Eq. 17). Fig. 2 depicts the normalized concentration of RH in the sensitivity analysis of some influencing rate constants. Additionally, checking of pseudofirst order kinetics is shown in the inset figures.

As observed, from Fig. 2, only few stages are important in the PMS/UV-C systems. There is no need of proposing a complex mechanism based on a high number of reactions. Analogously, negligible reactions should be discarded when reasoning the influence of some operating parameters. Insets in Fig. 2 present some deviations from real pseudo first order kinetics, although deviations are visible at relatively high RH conversions, that is why in most works pseudo first order kinetics correlate well with experimental data (use of few experimental data also hinders the error behind this assumption). Although not shown in Fig. 2, obviously the rate constants between radicals (sulfate and hydroxyl) and

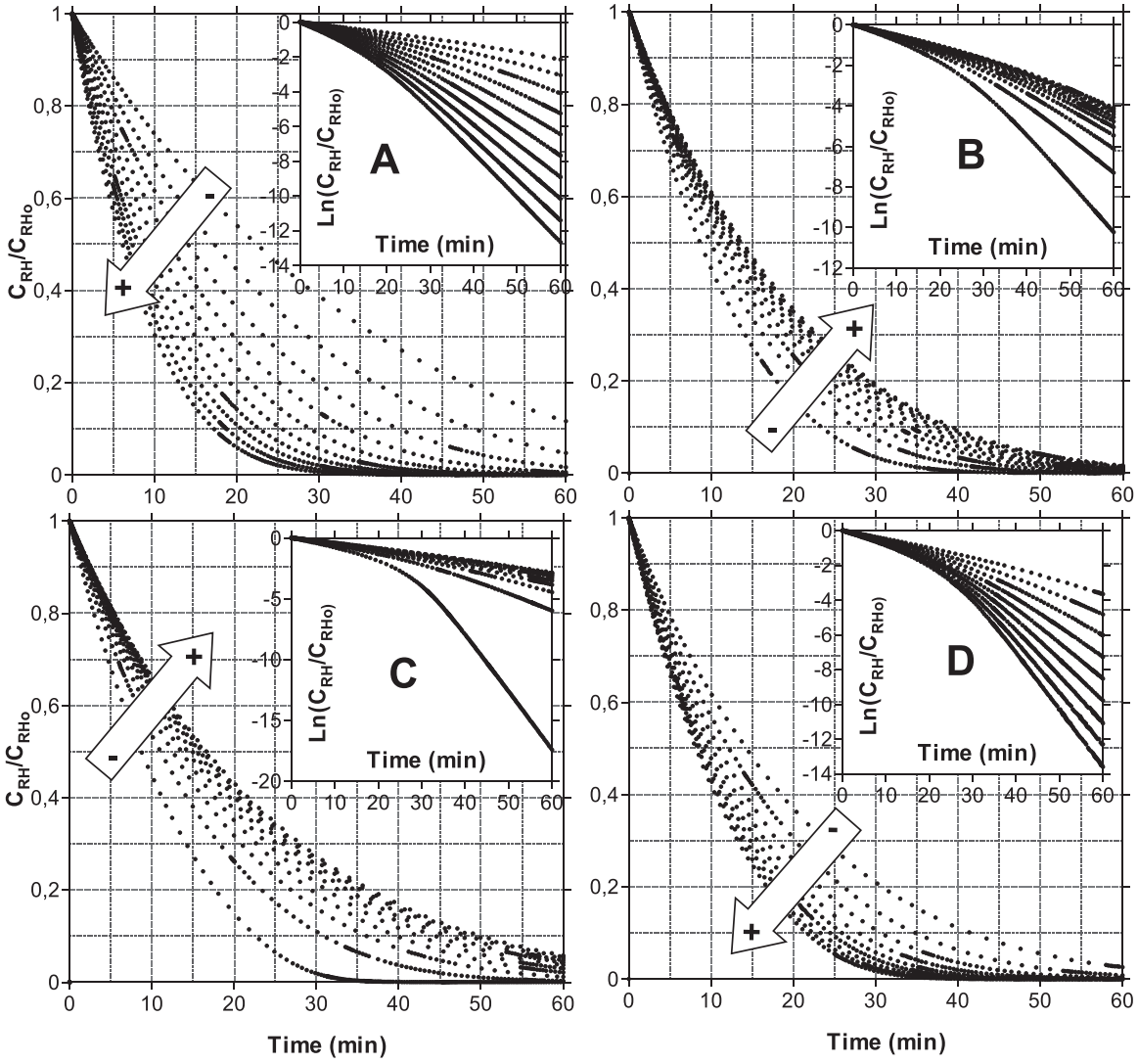

Fig. 2. Simulated removal of the generic compound RH by PMS activation under UV-C radiation. Evolution of RH concentration with time. Mechanism sensitivity analysis. A-Variation of UV-C intensity from 5×10^{-9} to 2×10^{-8} Einstein L^{-1} s^{-1}, B- Variation of k_7 from 5×10^{6} to 5×10^{7} M^{-1} s^{-1}, C- Variation of k_{13} from 1×10^{2} to 5×10^{3} s^{-1}, D- Variation of k_{15} from 5×10^{7} to 1×10^{9} M^{-1} s^{-1} Conditions: $C_{PMSo} = 1\times10^{-4}$ M, $C_{RHo} = 1\times10^{-7}$ M, $I_o = 1\times10^{-8}$ Einstein L^{-1} s^{-1}, L = 3 cm, pH = 7, T = 20 °C.

RH also influence the removal rate of the latter.

2.1.1. Influence of RH initial concentration

Besides the importance of using adequate rate constants, the set of reactions can be used to qualitatively assess the influence of reactions conditions. Given the relative simplicity of the mechanism, simulated results can only give an approximated idea of the real impact of studied parameters. Thus, for example, Fig. 3A shows the effect of the initial concentration of RH in the range 5.0–50.0×10^{-8} M. As experimentally observed in most of works, an increase in the initial concentration of the target compound leads to a decrease in the conversion rate (not in the removal rate). Results again deviate from linearity when plotting the natural logarithm of RH concentration versus time (see inset). From an exhaustive kinetic point of view, reaction order regarding RH concentration should be lower than 1.0, in no case should be taken as unity. Curves shown in Fig. 3 A were used to determine the reaction order regarding RH concentration by applying the differential methodology of kinetic parameter estimation. A reaction order of 0.79 + 0.001 was obtained with an acceptable consistency of this parameter. This reaction order corroborates the negative impact of increasing the initial RH concentration in its conversion. Few works have explained the negative effect of initial RH load from a kinetic point of view. Most authors simply justify this effect from a qualitative approach, i.e. as "the contaminant load is increased, the ratio radicals/target compound decreases and/or more intermediates are generated sequestering available radicals". Nevertheless, some attempts have been reported to account for the effect of initial contaminant load. Hence, Chen et al. (2007) assumed pseudo first order to occur in the system PMS/Co(II)/Acid Orange 7, however these authors derived an expression of the observed rate constant which was inversely proportional to initial target compound concentration.

2.1.2. Influence of PMS initial concentration

Another important parameter is the initial PMS concentration. Fig. 3B shows the influence of initial PMS concentration in the interval 3×10^{-5}-5×10^{-4} M. This species is responsible of radicals formation, and, obviously, should play a significant role. Hence, Zhang et al. (2021) report some pseudo first order rate constants that can be used to determine the dependency of the observed pseudo first order constant with PMS initial concentration of the type: $k_{obs} = k\ x C_{PMSo}^{\alpha}$ with $\alpha = 1.4$. Wang's work (Wang et al., 2018) leads to a lower value of $\alpha = 0.3$ while Rehman data (Rehman et al., 2018) resulted in $\alpha = 0.91$. Liang and Fu (2021) reported a value of 0.36 when treating Rhodamine B. Similarly to Ao and Liu (2017), Golshan et al. (2018) claims a linear relationship between k_{obs} and initial PMS concentration with slope = 0.64.

The apparent kinetics deduced from a n-th order general kinetic expression leads to the integrated expression (PMS concentration remains constant):

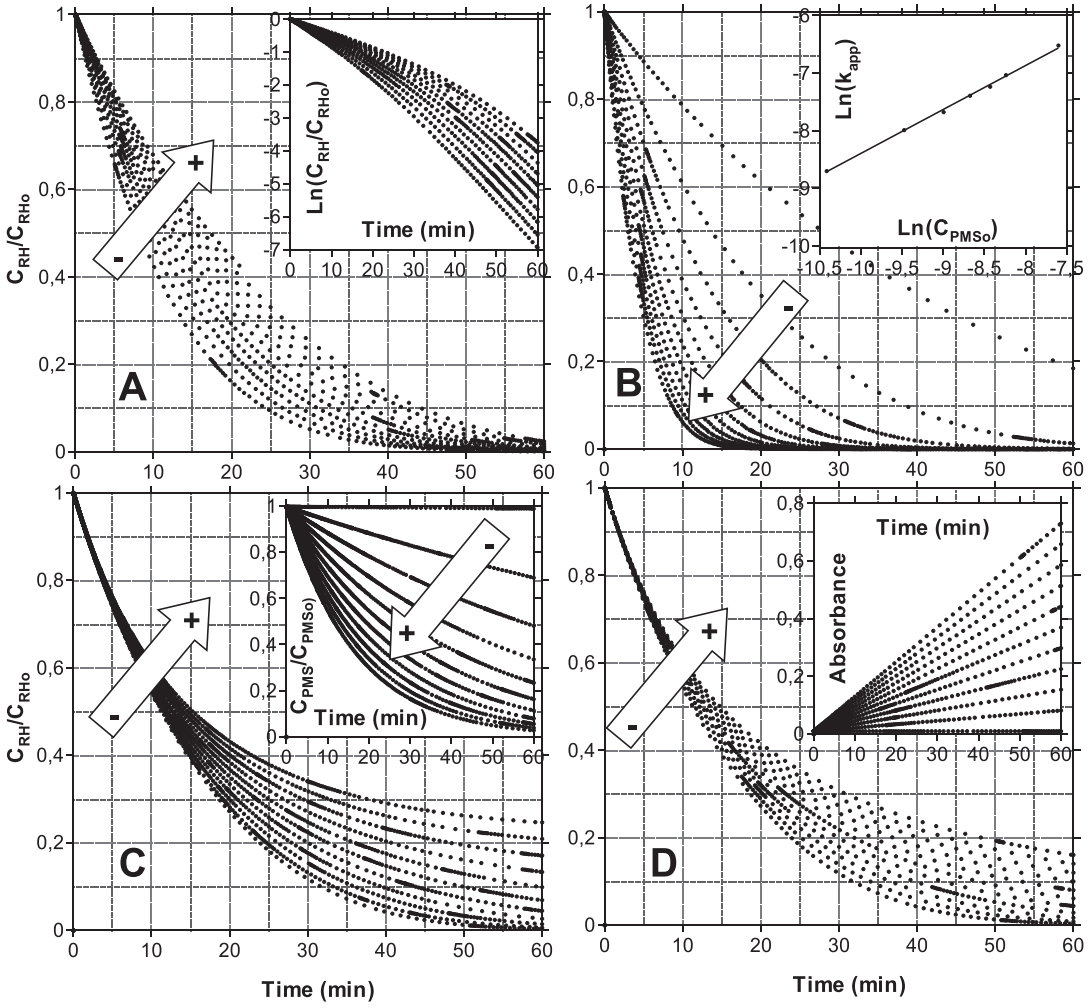

Fig. 3. Simulated removal of the generic compound RH by PMS activation under UV-C radiation. Evolution of RH concentration with time. Operating parameters influence. A-Variation of initial concentration of RH in the range 5.0–50.0×10^{-8} M, B- Variation of initial PMS concentration from 3 × 10^{-5} to 5 × 10^{-4} M, C-Variation of k_{40} from 0.0 to 1.0×10^{-3} s^{-1}, D- Linear variation of absorbance from 0.01 at time= 0. General conditions: $C_{PMSo} = 1 \times 10^{-4}$ M, $C_{RHo} = 1 \times 10^{-7}$ M, $I_o = 1 \times 10^{-8}$ Einstein L^{-1} s^{-1}, L = 3 cm, pH = 7, T = 20 ºC, Absorbance= 0.01.

$$\frac{1}{C_{RH}^{n-1}} = \frac{1}{C_{RH_o}^{n-1}} + (n-1) \times k_{app} \times t \quad (41)$$

By using a value of n = 0.8 (deduced from data in Fig. 3A), a plot of $\ln(k_{app})$ obtained from theoretical profiles in Fig. 3B versus $\ln(C_{PMSo})$ led to a straight line of slope 0.77 (inset in Fig. 3B), confirming the positive effect of initial PMS concentration.

No scavenging effects of high concentrations of PMS could be derived from the proposed mechanism. However, literature offers a variety of situations. For instance, Shad and collaborators (Shad et al., 2020) found no negative effects of increasing PMS concentrations when oxidizing sulfadimethoxine by UV-C/PMS. Contrarily, Kanjal report an optimum dosage in oxidant load when treating methotrexate with the same system (Kanjal et al., 2020). Numerous examples can be found defending the absence of PMS scavenging effects (Ao and Liu, 2017; Chen et al., 2014; Hu et al., 2019; Luo et al., 2015; Qi et al., 2013; Rehman et al., 2018; Yang et al., 2010) or the opposite (Ahmadi and Ghanbari, 2018; Z. Huang et al., 2021; Y. Huang et al., 2021; Rodríguez-Narvaez et al., 2020; Tang et al., 2021). Moreover, some authors claim the existence of PMS scavenging effect when no positive or negative influence is obtained above a certain limit. The mechanism of reactions used leads to an analogous result, with no significant improvement as the PMS approaches high values. The negative influence of PMS excess commonly attributed to radical scavenging, can also be the result of the inefficient decomposition of the peroxide (Rivas and Solís, 2018), which is normally proportional to PMS concentration when the oxidant is overdosed or locally in excess (see Eq. 40). Inefficient decomposition of hydrogen peroxide has also been suggested in Fenton processes (Rivas et al., 2005, 2003, 2002). Fig. 3C shows the influence of the value of the inefficient PMS decomposition rate constant in the range $0–10^{-3}\ s^{-1}$. Also, the inset of this figure depicts the evolution of PMS which is significantly affected by this parameter. Under this scenario, if PMS concentration significantly decreases, general kinetic expressions such as Eq. (39) should be revised (this expression has been obtained based on the negligible change in PMS concentration). Experimental PMS data collected during runs can bring to light the occurrence of this reaction.

$$HSO_5^- \rightarrow SO_4^{2-} + 1/2O_2 + H^+ \quad k = ?s^{-1} \quad (42)$$

2.1.3. Influence of absorbance evolution in irradiated systems

Another parameter that can affect the performance of irradiated PMS is the evolution of medium absorbance as the oxidation progresses. Fig. 3D illustrates the influence of absorbance evolution of the water matrix from 0.01 by considering a linear increase of this parameter with time. The inset depicts the linear increase of absorbance. Clearly, as the medium absorbance increases, an inner filter effect is experienced resulting in less radiation trapped by PMS. Photolysis of PMS is directly related to radical formation and, consequently to RH abatement.

2.1.4. Influence of generated intermediates

Another aspect in the presented mechanism that partially limits its validity is the role played by intermediates. It is obvious that generated intermediates affect absorbance evolution, compete for radicals and/or light with target contaminants or even can serve as radical promoters or photosensitizers. Knowing the number and nature of reaction intermediates is almost an impossible task. Some authors propose alternative strategies to account for intermediates influence (Solís et al., 2020). Hence, Chen et al. (2007) make an estimation of intermediates by just subtracting the time concentration of the target compound (acid orange 7) to the initial concentration. Thus, the stoichiometric coefficient is 1:1 with a reactivity of intermediates towards radicals similar to that of the parent compound. This approach has been applied in the theoretical results presented in Fig.s 1–3. Other possible strategies to face the role played by intermediates is to consider the generation of different fractions of intermediates with different reactivities and stoichiometric coefficients. This methodology has been adopted in the ozonation of fluorene (Rivas et al., 2006), or even in the simulation of the total organic carbon (TOC) in photocatalytic ozonation systems (Figueredo et al., 2020). Fig. 4A shows the influence of intermediates based on distinct hypothesis. Dotted lines correspond to formation from only one reacting intermediate up to four intermediates generated in series, with 1:1 stoichiometric factor, and reactivity towards radicals similar to RH. The scheme would be:

$$RH \xrightarrow{HO^\bullet/SO_4^{-\bullet}} P \xrightarrow{HO^\bullet/SO_4^{-\bullet}} P1 \xrightarrow{HO^\bullet/SO_4^{-\bullet}} P2 \xrightarrow{HO^\bullet/SO_4^{-\bullet}} P3 \xrightarrow{HO^\bullet/SO_4^{-\bullet}} P4 \quad (43)$$

As observed in Fig. 4A, differences are not especially significant. However, frequently after oxidation, scission of molecules may occur, so stoichiometric coefficients would be higher than unity. Solid line in Fig. 4A simulates the case where one mol of P generates 2 moles of P1, P1 generates 2 moles of P2 and so on. Finally, the dashed line considers a similar case with the stoichiometry being 5.

As inferred from Fig. 4A, as the number of intermediates is increased two degradation regions with different RH depletion rates appear. This is a typical behavior. Some authors take into account the presence of two different stages in the kinetic analysis of results (Wu et al., 2021; Chu et al., 2021). Also as inferred from Fig. 4A, when intermediates are taken into account, the system apparently approaches first order kinetics. The concave curves obtained by plotting the natural logarithm of normalized RH concentration versus time, initially obtained, tend to become straight lines. However, as more intermediates are considered, linearity is again lost, and convex curves are obtained (see inset in Fig. 4A). Deviation of first order kinetics are corroborated if runs at different initial RH concentration are simulated (Fig. 4B).

2.1.5. Influence of water matrix

Natural organic matter: Natural organic matter (NOM), and in general total organic carbon (TOC) content in water, influences the efficacy of PMS based technologies. The way NOM affects the process might advance in the positive or negative direction (Hu and Long, 2016; Canonica and Schönenberger, 2019). In the first case, the presence of quinone-type compounds can activate PMS decomposition. Zhou et al. (2017, 2015) claim the enhancement of reaction 44 due to the presence of benzoquinone through formation of a dioxirane intermediate. $^1O_2$ is a selective oxidant showing high reactivity towards electron-rich compounds.

$$HSO_5^- + SO_5^{2-} \rightarrow HSO_4^- + SO_4^{2-} + O_2^1 \quad k = 0.2 M^{-1}s^{-1} \quad (44)$$

Additionally, other authors report the positive influence of certain compounds in metal catalyzed PMS decomposition. Chen et al. (2019) reports the beneficial action of small organic acids presence in the system Co(II)/PMS by improving the catalytic activity of Co(II) in PMS decomposition, and the increased reduction of Co(III) to Co(II) due to electron donating capability. The influence of organics nature in the Co(II)/Co(III) redox cycle in the presence of PMS has already been suggested in the modelling of the Co(II)/PMS system (Rivas et al., 2012). This influence has also been observed in the enhancement of the Fe(III) reduction to Fe(II) in Fentonś chemistry due to the reaction of generated semiquinone radicals with ferric iron (Chen and Pignatello, 1997). In the presence of radiation, sometimes NOM can serve as photosensitizer. The negative impact of NOM or TOC comes from their radical scavenging nature (likely more pronounced towards $HO^\bullet$ than $SO_4^{-\bullet}$). NOM exhibits rate constants with $HO^\bullet$ and $SO_4^{-\bullet}$ radicals in the order $1.6–3.3\times10^8$ and $2.5–8.1 \times 10^7\ M^{-1}s^{-1}$, respectively (Lee et al., 2020). The positive impact of NOM can only be experimentally assessed, and the normal effect is expected to be as radical scavenger according to reactions 45 and 46.

$$RH + SO_4^{-\bullet} \rightarrow \text{Intermediate} + SO_4^{2-}\ k = 2{\cdot}5–8{\cdot}1 \times 10^7\ M^{-1}s^{-1} \quad (45)$$

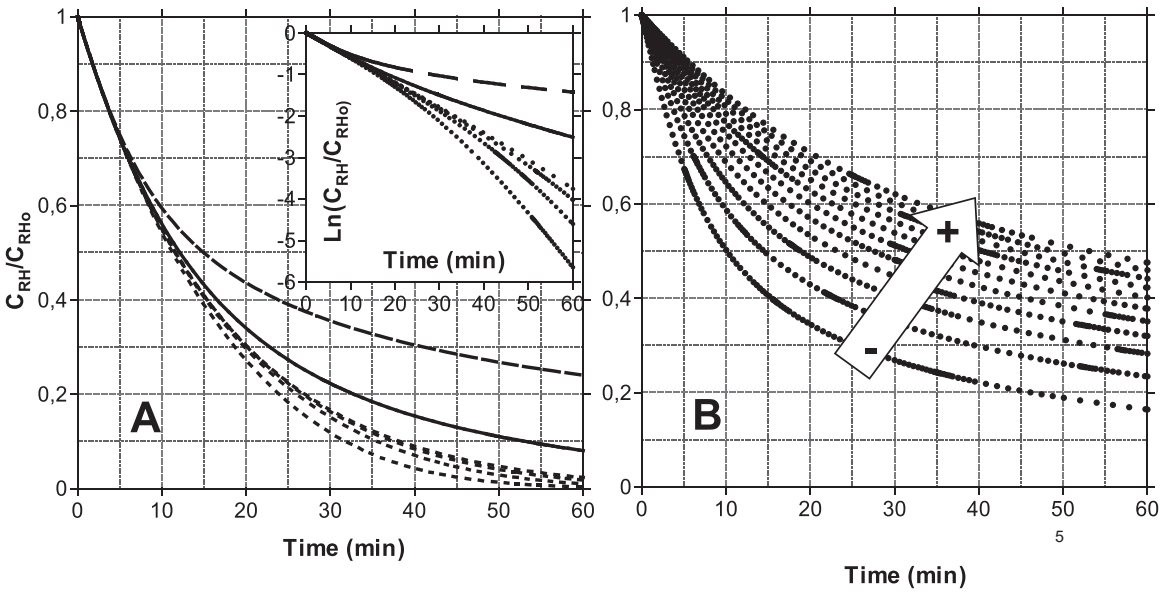

Fig. 4. Simulated removal of the generic compound RH by PMS activation under UV-C radiation. Evolution of RH concentration with time. Intermediates influence. A- Dotted lines: In series formation of 1, 2, 3, and 4 intermediates with stoichiometry 1:1, Solid line: In series formation of 4 intermediates with stoichiometry 1:2, Dashed line: In series formation of 4 intermediates with stoichiometry 1:5. B- Influence of initial RH concentration (5×10^{-8} – 5×10^{-7} M) for the case of formation of 4 intermediates with stoichiometry 1:5. General conditions: $C_{PMSo} = 1\times10^{-4}$ M, $C_{RHo} = 1\times10^{-7}$ M, $I_o = 1\times10^{-8}$ Einstein L^{-1} s^{-1}, L = 3 cm, pH = 7, T = 20 °C, Absorbance= 0.01 (reactivity of intermediates with radicals similar to RH).

$$RH + HO^{\bullet} \rightarrow \text{Intermediate} + HO^{-}\ k = 1{\cdot}6\text{–}3{\cdot}3\times10^{8}\ M^{-1}s^{-1} \quad (46)$$

The theoretical influence that TOC/NOM exerted in RH removal was studied by considering rate constants of the organic matter with hydroxyl and sulfate radicals of 2×10^{8} and 5×10^{7} $M^{-1}s^{-1}$, respectively. Initial TOC was set to 5×10^{-5} M (around 0.6 ppm). Fig. 5A shows the evolution of RH at different concentrations of initial TOC from 0 to 10^{-4} M. Additionally, Figs. 5B and C reveal the effect of the radical rate constants from 1.0×10^{6} to 4×10^{8} $M^{-1}s^{-1}$ in the case of the reaction of TOC with $HO^{\bullet}$, and from 1.0×10^{6} to 1×10^{8} $M^{-1}s^{-1}$ in the case of the reaction of TOC with $SO_4^{-\bullet}$.

As inferred from Fig. 5, water matrix in terms of organic matter content plays a significant role due to trapping of reactive radicals even at concentrations as low as one ppm. Theoretical profiles shown in Fig. 5A do not take into account that the negative influence can even be more pronounced if TOC/NOM absorbs radiation impeding PMS decomposition, i.e. the inner filter effect (Lutze et al., 2015). Moreover, NOM can also be adsorbed onto heterogeneous catalysts deactivating the capacity of the solid in heterogenous catalytic or photocatalytic processes (Ren et al., 2018). As expected, the reactivity of the organics (TOC/NOM) present in the water bulk substantially alters the abatement extent and rate of RH (Figs. 5B and C). The role played by NOM and the mode of interference in the process must experimentally be acquired previously to propose an adequate system model.

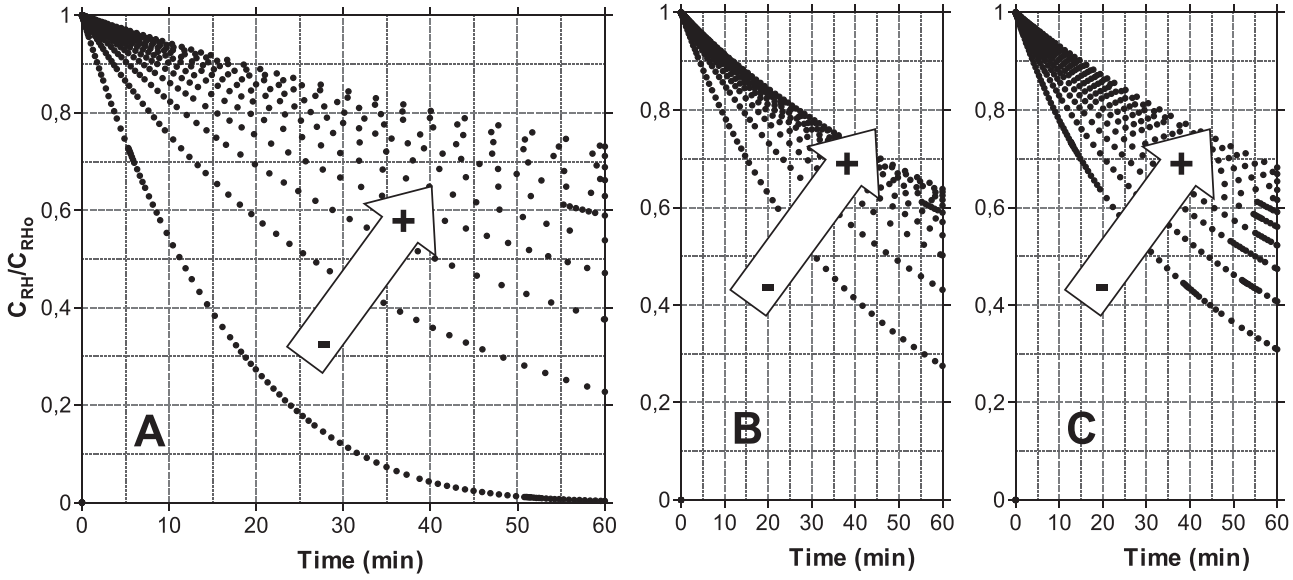

Fig. 5. Simulated removal of the generic compound RH by PMS activation under UV-C radiation. Evolution of RH concentration with time. A- Effect of initial TOC influence from 0 to 10^{-4} M. B- Influence of rate constant of TOC with HO• (1.0×10^{6} to 4×10^{8} $M^{-1}s^{-1}$), C- Influence of rate constant of TOC with $SO_4^{-\bullet}$ (1.0×10^{6} to 1×10^{8} $M^{-1}s^{-1}$). General conditions: $C_{PMSo} = 1\times10^{-4}$ M, $C_{RHo} = 1\times10^{-7}$ M, $I_o = 1\times10^{-8}$ Einstein L^{-1} s^{-1}, L = 3 cm, pH = 7, T = 20 °C, Absorbance= 0.01, $C_{TOCo} = 5\times10^{-5}$ M.

2.1.6. Influence of water matrix

Inorganic anions: Real wastewaters commonly present a relatively important load in inorganic salts. Accordingly anions such as Cl^-, HCO_3^-, NO_3^-, PO_3^{3-}, etc. are normally present. These species not only can be adsorbed onto solid catalysts interfering catalytic or photocatalytic processes, but also can trap radicals initiating additional reaction pathways, with variable effects, depending on the nature of water matrix constituents.

In the case of chloride, formation of chlorine has been detected by direct oxidation in the presence of PMS (Fortnum et al., 1960; Rivas and Solís, 2018). The following set of reactions is possible (Wu et al., 2019; Matthew and Anastasio, 2006) with k-units in M and s:

$$Cl^- + HSO_5^- \rightarrow HClO + SO_4^{2-} \quad k = 1.87{\cdot}10^{-3} \tag{47}$$

$$HClO \rightleftarrows ClO^- + H^+ \quad k = 1.6{\cdot}10^3, k- = 5.0{\cdot}10^{10} \tag{48}$$

$$\left.\begin{array}{c} HClO/ClO^- \\ Cl_2 \\ HClO^{\bullet-}/ClO^{\bullet} \\ Cl^{\bullet} \\ Cl_2^{\bullet-} \\ Cl_3^- \\ Cl_2O_2 \\ HClO_2/ClO_2^- \\ ClO_2^{\bullet} \\ ClO_3^- \end{array}\right\} + RH \rightarrow Intermediate(P) \quad k = ? \tag{49}$$

$$Cl^- + HO^{\bullet} \rightleftarrows HClO^{\bullet-} \quad k = 4.3{\cdot}10^9, k- = 6.1{\cdot}10^9 \tag{50}$$

$$Cl^- + SO_4^{\bullet-} \rightleftarrows Cl^{\bullet} + SO_4^{2-} \quad k = 3.0{\cdot}10^8, k- = 2.5{\cdot}10^8 \tag{51}$$

$$HClO^{\bullet-} + H^+ \rightarrow Cl^{\bullet} + H_2O \quad k = 2.0{\cdot}10^{10} \tag{52}$$

$$HClO^{\bullet-} + Cl^- \rightarrow Cl_2^{\bullet-} + OH^- \quad k = 1.0{\cdot}10^4 \tag{53}$$

$$Cl^{\bullet} + HSO_4^- \rightarrow HCl + SO_4^{\bullet-} \quad k = 2.5{\cdot}10^8 \tag{54}$$

$$Cl^{\bullet} + SO_4^{2-} \rightarrow Cl^- + SO_4^{\bullet-} \quad k = 2.5{\cdot}10^8 \tag{55}$$

$$Cl^{\bullet} + H_2O \rightarrow HClO^{\bullet-} + H^+ \quad k = 6.5{\cdot}10^2 \tag{56}$$

$$Cl^{\bullet} + OH^- \rightarrow HClO^{\bullet-} \quad k = 1.8{\cdot}10^{10} \tag{57}$$

$$Cl^{\bullet} + Cl^- \rightarrow Cl_2^{\bullet-} \quad k = 8.5{\cdot}10^9 \tag{58}$$

$$Cl^{\bullet} + Cl^{\bullet} \rightarrow Cl_2 \quad k = 8.8{\cdot}10^7 \tag{59}$$

$$Cl^{\bullet} + ClO^- \rightarrow ClO^{\bullet} + Cl^- \quad k = 8.3{\cdot}10^9 \tag{60}$$

$$Cl^{\bullet} + HClO \rightarrow ClO^{\bullet} + Cl^- + H^+ \quad k = 3.0{\cdot}10^9 \tag{61}$$

$$Cl^{\bullet} + H_2O_2 \rightarrow HO_2^{\bullet} + Cl^- + H^+ \quad k = 2.0{\cdot}10^9 \tag{62}$$

$$Cl_2^{\bullet-} \rightarrow Cl^{\bullet} + Cl^- \quad k = 5.0\ 10^3 \tag{63}$$

$$Cl_2^{\bullet-} + Cl_2^{\bullet-} \rightarrow Cl^{\bullet} + Cl^- + Cl_2 \quad k = 6.4\ 10^9 \tag{64}$$

$$Cl_2^{\bullet-} + Cl^{\bullet} \rightarrow Cl^- + Cl_2 \quad k = 2.1\ 10^9 \tag{65}$$

$$Cl_2^{\bullet-} + HO_2^2 \rightarrow 2Cl^- + H^+ + HO_2^{\bullet} \quad k = 1.4\ 10^5 \tag{66}$$

$$Cl_2^{\bullet-} + HO_2^{\bullet} \rightarrow 2Cl^- + H^+ + O_2 \quad k = 3.0\ 10^9 \tag{67}$$

$$Cl_2^{\bullet-} + O_2^{\bullet-} \rightarrow 2Cl^- + O_2 \quad k = 2.0\ 10^9 \tag{68}$$

$$Cl_2^{\bullet-} + HO^{\bullet} \rightarrow HClO + Cl^- \quad k = 1.0\ 10^9 \tag{69}$$

$$Cl_2^{\bullet-} + OH^- \rightarrow HClO^{\bullet-} + Cl^- \quad k = 4.5\ 10^7 \tag{70}$$

$$Cl_2 + Cl^- \rightleftarrows Cl_3^- \quad k = 2.0\ 10^4, k- = 1.0\ 10^5 \tag{71}$$

$$Cl_2 + HO_2^{\bullet} \rightarrow Cl_2^{\bullet-} + O_2 + H^+ \quad k = 1.0\ 10^9 \tag{72}$$

$$Cl_2 + O_2^{\bullet-} \rightarrow Cl_2^{\bullet-} + O_2 \quad k = 1.0\ 10^9 \tag{73}$$

$$Cl_2 + H_2O_2 \rightarrow O_2 + 2Cl^- + 2H^+ \quad k = 1.3\ 10^4 \tag{74}$$

$$Cl_3^- + HO_2^{\bullet} \rightarrow Cl_2^{\bullet-} + Cl^- + H^+ + O_2 \quad k = 1.0\ 10^9 \tag{75}$$

$$Cl_3^- + O_2^{\bullet-} \rightarrow Cl_2^{\bullet-} + Cl^- + O_2 \quad k = 3.8\ 10^9 \tag{76}$$

$$H_2O_2 + HClO \rightarrow O_2 + Cl^- + H^+ + H_2O \quad k = 1.0{\cdot}10^4 \tag{77}$$

$$HO^{\bullet} + HClO \rightarrow ClO^{\bullet} + H_2O \quad k = 2.0{\cdot}10^9 \tag{78}$$

$$O_2^{\bullet-} + HClO \rightarrow Cl^{\bullet} + OH^- + O_2 \quad k = 7.5{\cdot}10^6 \tag{79}$$

$$HO_2^{\bullet} + HClO \rightarrow Cl^{\bullet} + H_2O + O_2 \quad k = 7.5{\cdot}10^6 \tag{80}$$

$$H_2O_2 + ClO^- \rightarrow O_2 + Cl^- + H_2O \quad k = 1.7{\cdot}10^5 \tag{81}$$

$$HO^{\bullet} + ClO^- \rightarrow ClO^{\bullet} + OH^- \quad k = 8.8{\cdot}10^9 \tag{82}$$

$$O_2^{\bullet-} + ClO^- + H_2O \rightarrow Cl^{\bullet} + 2OH^- + O_2 \quad k = 2.0{\cdot}10^8 \tag{83}$$

$$HOCl + H^+ + Cl^- \rightleftarrows Cl_2 + H_2O \quad k = 18000, k- = 0.4 \tag{84}$$

$$ClO^{\bullet} + ClO_2^- \rightarrow ClO^- + ClO_2^{\bullet} \quad k = 9.4{\cdot}10^8 \tag{85}$$

$$HO^{\bullet} + ClO_2^- \rightarrow OH^- + ClO_2^{\bullet} \quad k = 1.0{\cdot}10^9 \tag{86}$$

$$HO^{\bullet} + ClO_2^{\bullet} \rightarrow H^+ + ClO_3^- \quad k = 4.0{\cdot}10^9 \tag{87}$$

$$ClO_2^{\bullet} + SO_4^{\bullet-} + H_2O \rightarrow 2H^+ + ClO_3^- + SO_4^{2-} \quad k = 8.2{\cdot}10^9 \tag{88}$$

$$2ClO^{\bullet} + H_2O \rightarrow 2H^+ + ClO_2^- + ClO^- \quad k = 2.5{\cdot}10^9 \tag{89}$$

$$2ClO^{\bullet} \rightarrow Cl_2O_2 \quad k = 2.5{\cdot}10^9 \tag{90}$$

$$2ClO^{\bullet} + OH^- \rightarrow ClO^- + ClO_2^- + H^+ \quad k = 2.5{\cdot}10^9 \tag{91}$$

$$Cl_2^{\bullet-} + ClO_2^- \rightarrow ClO_2^{\bullet} + 2Cl^- \quad k = 1.3{\cdot}10^8 \tag{92}$$

$$ClO^{\bullet} + OH^{\bullet} \rightarrow ClO_2^{\bullet-} + H^+ \quad k = 1.0{\cdot}10^9 \tag{93}$$

$$ClO_2^{\bullet} + HO_2^{\bullet-} \rightarrow HClO_2 + O_2 \quad k = 1.0{\cdot}10^6 \tag{94}$$

$$ClO_2^{\bullet} + O_2^{\bullet-} \rightarrow ClO_2^- + O_2 \quad k = 3.0{\cdot}10^9 \tag{95}$$

$$ClO_2^{\bullet} + HO_2^- \rightarrow ClO_2^- + HO_2^{\bullet} \quad k = 8.0{\cdot}10^4 \tag{96}$$

$$HClO_2 \rightleftarrows ClO_2^- + H^+ \quad K = 1.0{\cdot}10^{-2} \tag{97}$$

Impact of chloride in PMS based technologies highly depends on the key reaction 49, i.e. the reactivity of RH with oxidant species generated in the presence of Cl^-. A first attempt to understand Cl^- effect was carried out by assuming no reactivity at all of RH with chloride derived oxidant (ClDOx) species. Fig. 6 shows the simulated theoretical normalized RH concentration in the presence of Cl^- in the range $0 - 4{\times}10^{-4}$ M (pH 3, 7 and 11).

As observed, in the absence of reaction of RH with ClDOx, two main

conclusions can be derived. On one hand, in no case Cl^- could promote/activate the abatement of RH, the inhibition of RH oxidation is clearly stated, even for chloride concentrations as low as 14 ppm. On another hand, pH plays a significant role in the system efficiency (even in the absence of chloride). Consequently, the positive influence of Cl^- reported in some works must undoubtedly be the result of reaction 49 occurrence (simulation in Fig. 6 was obtained without considering reaction 49). Reactivity of ClDOx with organics highly depends on RH nature (Lei et al., 2019; Neta et al., 1988). Moreover, ClDOx can also interact with other inorganic species such as carbonates or metallic cations (i.e. Co (II)), complicating even more the mechanism. The relevance of the different ClDOx was theoretically obtained by conducting a sensitivity analysis of k_{49} values. Apparently, one of the influencing species is $Cl_2^{-\bullet}$ (rate constant k_{49} tested in the range $0–1\times10^9$ $M^{-1}s^{-1}$ in Fig. 7A), however the role played by this radical is controversial. Hence, Minakata et al. (2017) claim that the reactivity of the dichloride radical with organic compounds is negligible in the UV/chlorine system. Contrarily, Lei et al. (2019) report second order rate constants of $Cl_2^{-\bullet}$ with trace organic contaminants in the range 1×10^6-3×10^9 $M^{-1}s^{-1}$. Yuan et al. (2014) report the crucial role played by $Cl_2^{-\bullet}$ in the UV/Persulfate elimination of acid orange 7 in saline waters. Additionally, at pH 7 and considering the mechanism of reactions assumed, HClO concentration predominates over ClO^- (more than one order of magnitude). Under these circumstances, hypochlorous acid shows a higher oxidative capacity than hypochlorite. Fig. 7B shows the influence of the rate constant between HClO and RH in the interval $0–10^5$ $M^{-1}s^{-1}$. The effect of ClO^- rate constant in the same range of values is less pronounced. Fig. 7C depicts the effect of ClO^- rate constant in the range 0–5 10^6 $M^{-1}s^{-1}$. The rest of ClDOx other than $Cl_2^{-\bullet}$ or the couple HClO/ClO^- did have no effect or have residual influence on RH removal rate.

Another important inorganic species in radical based water treatments is the couple $HCO_3^-/CO_3^{=}$. In a first approach, the following reactions should be considered, mainly radical scavenging (Lee et al., 2020):

$$HCO_3^- + HO^\bullet \rightarrow CO_3^{-\bullet} + H_2O \quad k = 8.5\cdot10^6 \tag{98}$$

$$CO_3^{2-} + HO^\bullet \rightarrow CO_3^{-\bullet} + OH^- \quad k = 3.9\cdot10^8 \tag{99}$$

$$HCO_3^- + SO_4^{-\bullet} \rightarrow CO_3^{-\bullet} + SO_4^{2-} + H^+ \; k = 1.6 - 9.1\cdot10^6 \tag{100}$$

$$CO_3^{2-} + SO_4^{-\bullet} \rightarrow CO_3^{-\bullet} + SO_4^{2-} \quad k = 6.1\cdot10^6 \tag{101}$$

$$CO_3^{-\bullet} + CO_3^{-\bullet} \rightarrow CO_2 + CO_4^{2-} \; k = 2.0\cdot10^7 \tag{102}$$

$$HCO_3^- \rightleftarrows CO_3^{2-} + H^+ \; pK = 10.3 \tag{103}$$

$$H_2CO_3 \rightleftarrows HCO_3^- + H^+ \quad pK = 6.3 \tag{104}$$

(no scavenging reactions of carbonic acid is found in literature).

However, secondary reactions may play a significant role in the system. For instance, carbonate radicals can react with electron rich target compounds (Wojnárovits et al., 2020), natural organic matter, cations (especially important in Co(II) activated systems), etc.

$$CO_3^{-\bullet} + \begin{cases} RH \\ NOM \\ M^{+n} \end{cases} \rightarrow Products \quad k = ? \tag{105}$$

Additionally in the presence of chlorides, ClDOx can also generate carbonate radicals:

$$HCO_3^- + Cl^\bullet \rightarrow CO_3^{-\bullet} + H^+ + Cl^- \quad k = 0.8 - 2.2\cdot10^8 \tag{106}$$

$$HCO_3^- + Cl_2^{-\bullet} \rightarrow CO_3^{-\bullet} + H^+ + 2Cl^- \quad k = 1.6 - 5.0\cdot10^8 \tag{107}$$

Finally, some authors (Nie et al., 2019) claim the activation of PMS by carbonates to generate an oxidative mechanism based on the superoxide anion radical and singlet oxygen. Activation seems to be due to the high pH value rather than the presence of the carbonate anion. In this case, scavenging of these reactive oxygenated species by carbonates should also been considered.

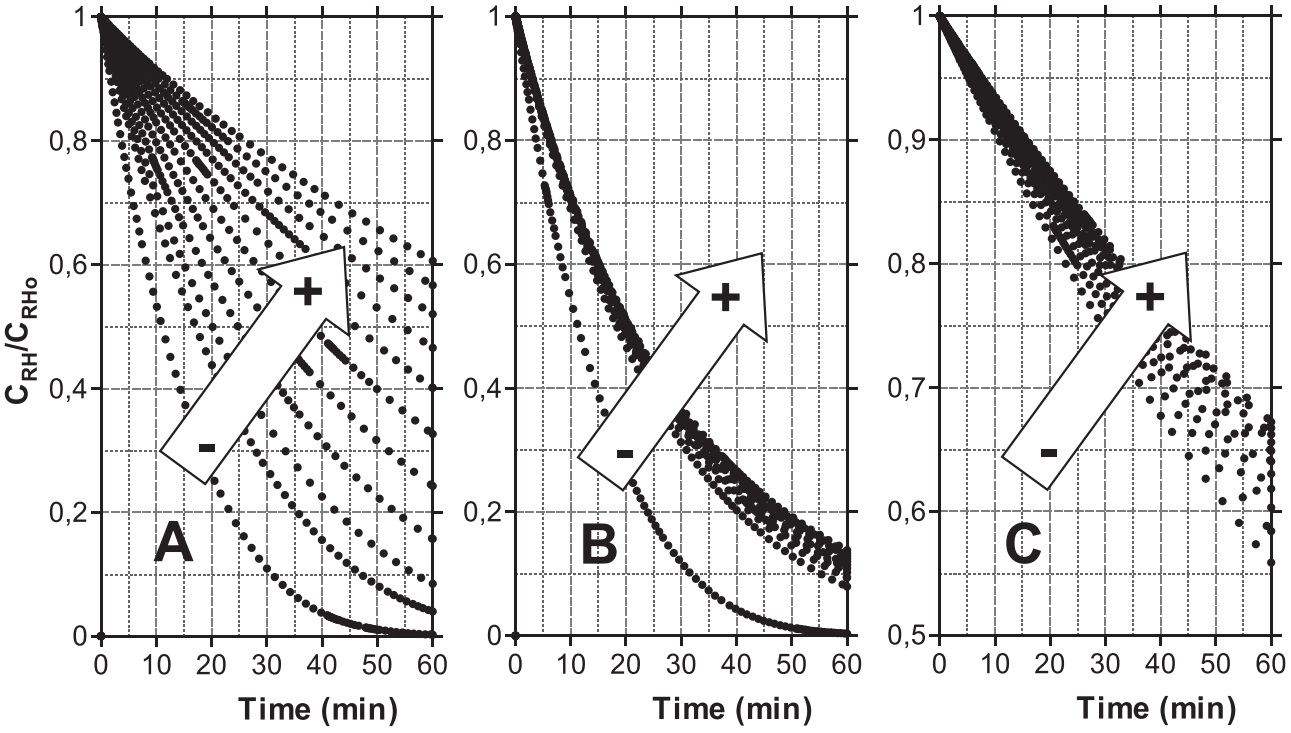

Fig. 6. Simulated removal of the generic compound RH by PMS activation under UV-C radiation. Evolution of RH concentration with time. Effect of initial Cl^- from 0 to 4 10^{-4} M at pH 3 (A), pH 7 (B) and pH 11 (C). General conditions: $C_{PMSo} = 1 \times 10^{-4}$ M, $C_{RHo} = 1 \times 10^{-7}$ M, $I_o = 1 \times 10^{-8}$ Einstein L^{-1} s^{-1}, L = 3 cm, T = 20 °C, Absorbance= 0.01.

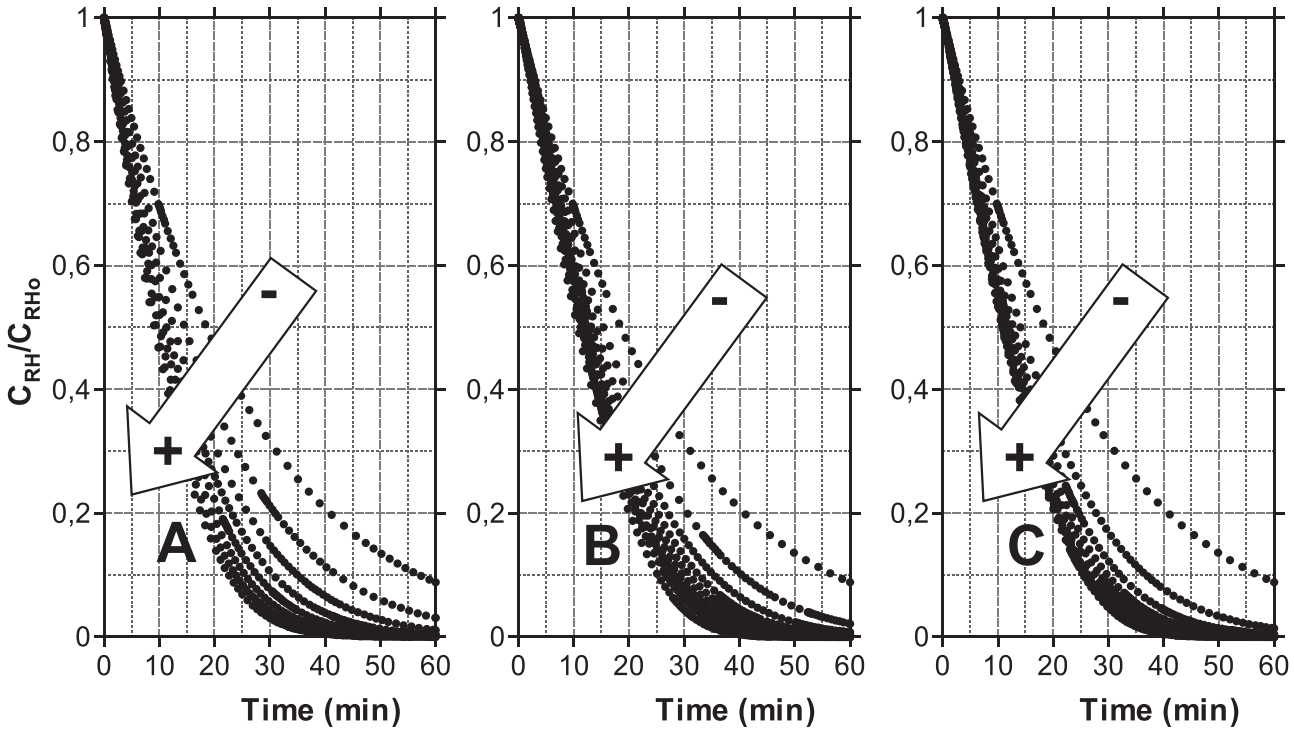

Fig. 7. Simulated removal of the generic compound RH by PMS activation under UV-C radiation. Evolution of RH concentration with time. Effect of ClDOx-RH rate constant value. A- RH-Cl_2^{-}• rate constant from 0 to 1.0×10^{9} $M^{-1}s^{-1}$; B- RH-HClO rate constant from 0 to 1.0×10^{5} $M^{-1}s^{-1}$; C- RH-ClO^{-} rate constant from 0 to 5.0×10^{6} $M^{-1}s^{-1}$. General conditions: $C_{PMSo} = 1 \times 10^{-4}$ M, $C_{RHo} = 1 \times 10^{-7}$ M, $I_o = 1 \times 10^{-8}$ Einstein L^{-1} s^{-1}, L = 3 cm, T = 20 ºC, Absorbance= 0.01, $C_{Cl\text{-}o} = 2.0\times10^{-4}$ M.

Reactions 98–107 were therefore introduced into the model. Fig. 8A shows the influence of alkalinity in the range 0–10^{-3} M in HCO_3^{-} when RH does not react with carbonate radicals (pH 7). As expected, the presence of carbonates significantly inhibits RH oxidation due to hydroxyl and sulfate radicals trapping. A lower inhibition was theoretically obtained at basic pH of 11, even though, at basic pH, conversion of sulfate radicals to hydroxyl radicals is favored. Almost no inhibition was determined at pH 3 due to displacement of equilibrium 104 to the left. In any case, depending on RH nature, reaction of target compounds with carbonate radicals may play an important role. Fig. 8B shows the simulated influence of the rate constant value between RH and carbonate radicals (from 0 to 5 10^{6} $M^{-1}s^{-1}$) for an initial HCO_3^{-}

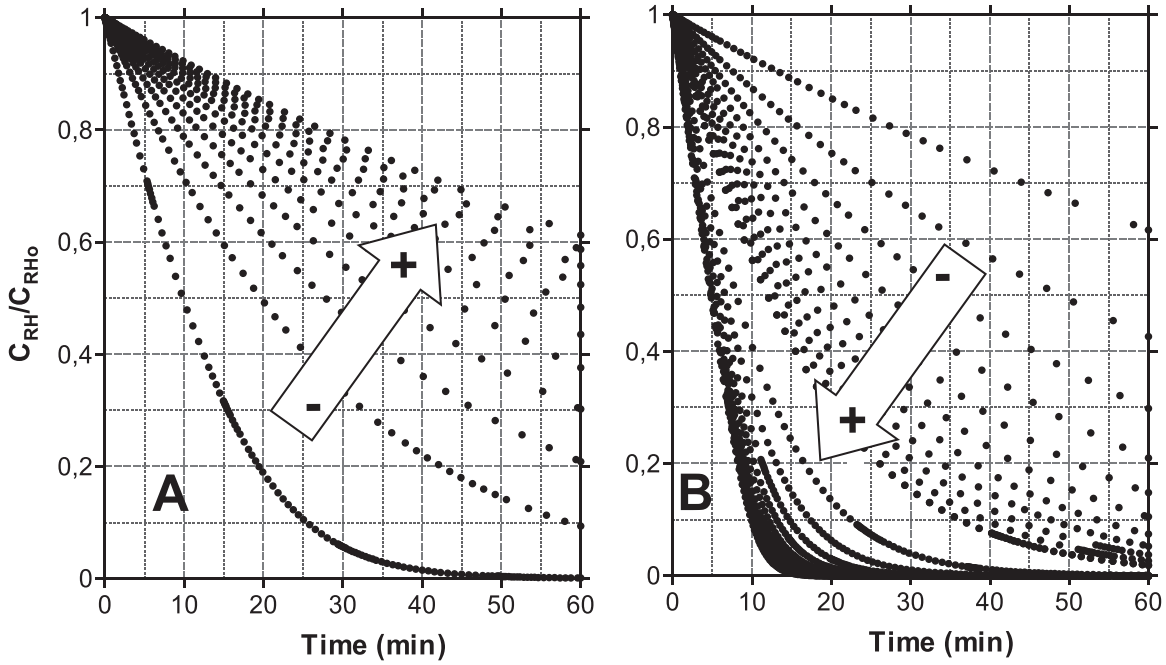

Fig. 8. Simulated removal of the generic compound RH by PMS activation under UV-C radiation. Evolution of RH concentration with time. Effect of carbonates. A-HCO_3^{-} concentration from 0 to 1.0×10^{-3} M (no reaction between RH and carbonate radicals); B- RH-CO_3^{-}• rate constant from 0 to 5.0×10^{6} $M^{-1}s^{-1}$. General conditions: $C_{PMSo} = 1 \times 10^{-4}$ M, $C_{RHo} = 1 \times 10^{-7}$ M, $I_o = 1 \times 10^{-8}$ Einstein L^{-1} s^{-1}, L = 3 cm, T = 20 ºC, Absorbance= 0.01, pH = 7, $C_{HCO3\text{-}o} = 1.0\times10^{-3}$ M.

concentration of 0.001 M at pH 7.

Fig. 8B sustains the positive effect of carbonates found by some authors when dealing with substances reactive to carbonate radicals. The extent of the positive effect will undoubtedly be related to the ratio of C_{RH}/ C_{HCO3-o} and the ratio of the constants with active radicals. The presence of chlorides influences the efficacy of the process through reactions 106 and 107. The overall effect will depend, besides of concentration, on the reactivity of target compounds with ClDOx and $CO_3^{-\bullet}$.

Other anions such as nitrites, phosphates, bromides, etc. can also interfere in the process. The influence of bromide is similar to chloride while in the presence of phosphates, $HPO_4^{=}$ has been reported to be able to decompose PMS to generate hydroxyl radicals (Duan et al., 2021).

2.1.7. Radical scavengers addition

It is of common practice to use specific substances to assess the role played by the different oxidant species in PMS based systems. Typically, scavengers of hydroxyl radicals, sulfate radicals, singlet oxygen and to a lesser extent perhydroxyl radicals are used. Hence, *tert*-butyl alcohol (t-BuOH) shows a relatively high reactivity towards hydroxyl radicals ($3.8–7.6{\cdot}10^8$ M^{-1} s^{-1}) and low rate constant with sulfate radicals ($4.0–9.1{\cdot}10^5$ M^{-1} s^{-1}), meanwhile ethanol (EtOH) can scavenge both hydroxyl radicals ($1.2-2.8{\cdot}10^9$ M^{-1} s^{-1}) and sulfate radicals ($1.6-7.7{\cdot}10^7$ M^{-1} s^{-1}). As a rule of thumb, when using these radical quenchers, no further considerations are taken into account, however, radical attack to scavengers can initiate a parallel route of ROS generation, including organic radicals (hydroxyalkyl or alkoxyl radicals), hydrogen peroxide and/or perhydroxyl radicals as it is the case of tBuOH, ethanol or 2-propanol (Rivas et al., 2015; Solís et al., 2020; Cederbaum et al., 1983).

Sodium azide is utilized as $^1O_2$ trapping agent in many works. However, scavengers are not completely specific towards one unique ROS. Hence NaN_3 reacts with hydroxyl and sulfate radicals with a rate constant of roughly $8.0{\times}10^{10}$ and $3.0{\times}10^9$ $M^{-1}s^{-1}$ (Shinohara et al., 1962; Neta et al., 1988). Additionally, 1,3-benzenedisulfonic acid, 4, 5-dihydroxy-, disodium salt (Tiron), is mainly used as hydroperoxyl radical trapping agent. Again, this substance is also capable of scavenging hydroxyl and sulfate radicals, so no reliable conclusions can be derived from its effect.

As an example, the effect of t-BuOH and EtOH in RH removal rate is simulated by addition of Eqs. (108–111) with units in $M^{-1}s^{-1}$:

$$HO^{\bullet} + tBuOH \rightarrow Products \quad k = 5{\cdot}10^8 \tag{108}$$

$$SO_4^{-\bullet} + tBuOH \rightarrow Products \quad k = 6{\cdot}10^5 \tag{109}$$

$$HO^{\bullet} + EtOH \rightarrow Products \quad k = 2{\cdot}10^9 \tag{110}$$

$$SO_4^{-\bullet} + EtOH \rightarrow Products \quad k = 4{\cdot}10^7 \tag{111}$$

Fig. 9 reveals how EtOH in the range $0–10^{-3}$ M inhibits RH oxidation to a higher extent than tBuOH for the same range of concentrations. Obviously, the scavenging effect will be directly related to the comparative reactivity of RH with sulfate and hydroxyl radicals. In the simulation, RH reactivity towards both radicals is similar.

Simulations shown in Figs. 1–9 have been obtained by considering PMS activation by UV radiation. Similar results, however, are expected if other activation stages are used. Some features associated to these other activation methos should be considered.

Hence, the other most popular method of homogeneous PMS activation is through Co(II) catalysis. In the latter case, values of rate constants for reactions 1–3 would significantly determine the kinetics of the process. The rest of influencing parameters should, a priori, present the same behavior than the UV activated process. When using metal cations as it is the case of Co(II), potential reactions that would oxidize Co(II) to Co(III) should also been considered. Amongst these reactions, besides the oxidation by hydroxyl and sulfate radicals (Eqs. 26 and 27), other potential routes of Co(II) transformation include the oxidation by carbonate radicals ($k = 2.8–4.4{\times}10^6$ $M^{-1}s^{-1}$), by hydrogen peroxide (Ling et al., 2010), oxidation by organic radicals, oxidation by ClDOx, precipitation by carbonates, etc. As mentioned previously, Eqs. 1–3 are crucial in the system and strongly depend on the cobalt complexing agents present/formed in solution. In the literature, distinct target compounds degradation profiles are found. For instance, in some cases,

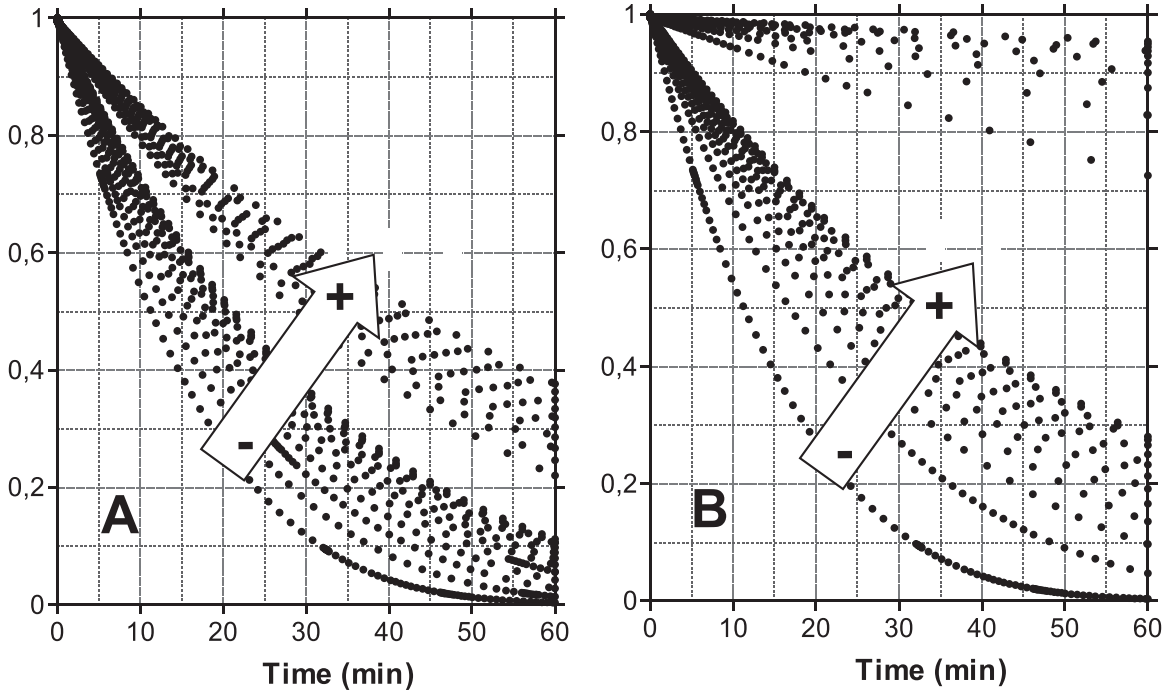

Fig. 9. Simulated removal of the generic compound RH by PMS activation under UV-C radiation. Evolution of RH concentration with time. Effect of radical scavengers. A- tBuOH concentration from 0 to $1.0{\times}10^{-3}$ M; B- EtOH concentration from 0 to $1.0{\times}10^{-3}$ M. General conditions: $C_{PMSo} = 1 \times 10^{-4}$ M, $C_{RHo} = 1 \times 10^{-7}$ M, $I_o = 1 \times 10^{-8}$ Einstein L^{-1} s^{-1}, L = 3 cm, T = 20 °C, Absorbance= 0.01, pH = 7.

the target compound shows a fast initial degradation leading thereafter to a halt period of limited or null removal. Since normally PMS is used in excess, this behavior seems to be associated to a limitation in Co(III) reduction (Eq. 3). In other situations, however, target compound are continuously degraded even when extremely low Co(II) concentrations are used (Huang et al., 2009). The different profiles experienced can be obtained by assigning diverse values to rate constants in Eqs. 1–3, i.e. the ratio Co(II) oxidation to Co(III) reduction. Fig. 10 reveals the influence of radicals formation (Eqs. 1 and 2) and Co(III) reduction (Eq. 3). In pure water, decomposition of PMS by cobalt obeys the following rate in s^{-1} (Kim and Edwards, 1995):

$$-\frac{dC_{PMS}}{dt} = k\frac{C_{PMS}C_{Co(II)}}{C_{H^+}} \quad k = 9.510^{-3} \tag{112}$$

The previous expression is a global equation including PMS scavenging by generated radicals and Co(III) reduction, however can give a generic idea of values of Eqs. (1–3) rate constants. Considering that the presence of complexing agents highly affects Eqs. (1–3) rates, for simulation purposes the generation of radicals through Eqs. (1 and 2) was assumed to have values in the range 10–100 $M^{-1}s^{-1}$ (similar to Fenton initiation stage) while Eq. (3) rate was varied to assess its influence.

Fig. 10 A simulates the case where trace amounts of Co(II) can degrade a generic compound RH with final conversions depending on the capability of Co(III) to be reduced, in this case, Eqs. (1 and 2) were given a rate constant of 100 $M^{-1}s^{-1}$ while reduction of Co(III) was varied in the interval 0–100 $M^{-1}s^{-1}$.

In other cases, however, when the conversion of RH reaches a maximum, Co(III) reduction is restricted and RH degradation is almost limited to Co(II) disappearance. Fig. 10B shows the case in which no reduction of Co(III) takes place at different concentrations of Co(II). A value of 10 $M^{-1}s^{-1}$ has been assumed for the rate constants that generate radicals while initial Co(II) concentration was varied from 1.0 10^{-8} to 2.0 10^{-7} M.

2.2. Heterogenous initiation reactions

Use of heterogenous catalysis in PMS activation is increasingly attracting the attention of researches. Several clear benefits such as easy separation of the catalyst, no need of homogenous metal catalyst recovery, and wider margin in operation parameters, especially pH, can be cited (Oh et al., 2016). Various works have dealt with the latest novelties in heterogeneous PMS catalysis (Ghanbari and Moradi, 2017; Giannakis et al., 2021; Oh et al., 2016; Hu and Long, 2016). These studies review the state of the art of different catalyst families, inquiring the main features of operating variables influence, reactive species determination, applications, etc. However, no especial attention has been paid to kinetic studies. An attempt was made by Oh et al. (2015) to propose a kinetic expression in the elimination of bisphenol A by $CuFe_2O_4$–Fe_2O_3. The equation took into account pH effects, and the protonation of the catalyst hydroxyl surface groups according to:

$$C_{RH} = C_{RH_o}\exp\left(\frac{k_{int}C_{Cat_o}}{k_{PMS}\left(K_{eq}C_{H^+}+1\right)}C_{PMS_o}\left(e^{-k_{PMS}t}-1\right)\right) \tag{113}$$

Where k_{int}, k_{PMS} and K_{eq} are the intrinsic, first order PMS decomposition rate constants and catalyst-proton equilibrium, respectively. C_i is concentration of species i (generic compound RH, catalyst and peroxymonosulfate), while the subindex "o" stands for initial conditions. The authors considered the surface reaction taking place on the solid surface (k_{int}) with first order regarding PMS, catalyst and target compound. However other scenarios may be encountered.

As a common practice, assessment of the performance of heterogeneous catalysis requires a previous study of the effect of mass transport on the overall kinetics (Sievers et al., 2016), both external and internal mass transfer limitations. Dependence of the observed reaction rate with temperature may serve as an indicative tool to determine if the process is diffusion limited. Processes controlled by diffusion of reactants towards the catalyst surface present low values of activation energy. If the limitation is external, a simple increase in the agitation speed of slurry reactors should decrease this negative effect (or volumetric flow in other

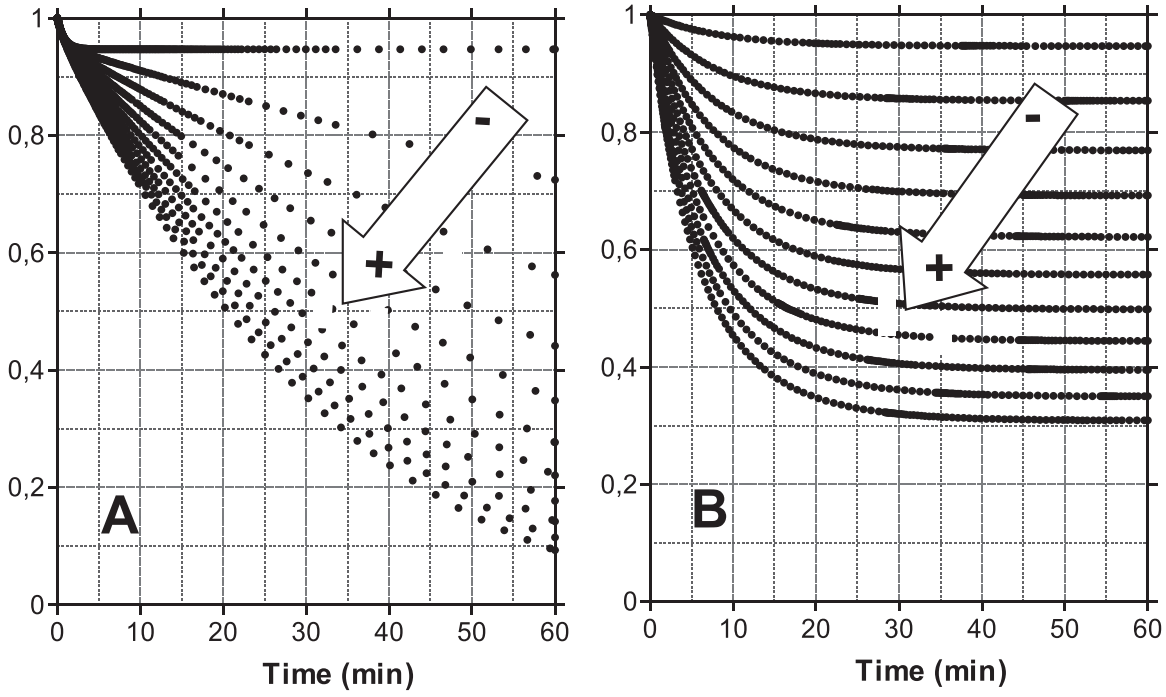

Fig. 10. Simulated removal of the generic compound RH by PMS activation with Co(II). Evolution of RH concentration with time. Effect of Co(III) reduction rate. A- $C_{Co(II)o} = 1.0\times10^{-8}$ M, $k_1 = k_2 = 100$ $M^{-1}s^{-1}$, k_3 variation from 0 to 100 $M^{-1}s^{-1}$; B- $k_1 = k_2 = 10$ $M^{-1}s^{-1}$, $k_3 = 0$ $M^{-1}s^{-1}$, $Co(II)_o$ variation from 0 to 2.0×10^{-7} M. General conditions: $C_{PMSo} = 1\times10^{-4}$ M, $C_{RHo} = 1\times10^{-7}$ M, T = 20 ºC, pH = 4.

configurations). The existence of internal transport limitations is normally determined through the calculation of distinct criteria. One of the most popular criteria is the dimensionless Weisz-Prater parameter defined as:

$$\Phi_{W-P} = \frac{r_{obs} R_{Cat}^2}{C_{RH}^{Surface} D_{eff}} \quad (114)$$

Where r_{obs} is the observed RH elimination rate, R_{Cat} is the catalyst particle radius, $C_{RH}^{Surface}$ is the concentration of RH at the external catalyst surface and D_{eff} is the effective diffusivity of compound RH (different from bulk diffusivity). The critical value of Φ_{W-P}depends on reaction order in the interval 0.3 – 6.0 (for typical reaction order from 0 to 2). Accordingly, no mass transfer scenarios are assumed for Φ_{W-P} values below 0.3 while values above 6.0 indicates the existence of mass transport limitations. A unique frontier value of 1.0 is however normally used. Effective diffusivity can be calculated by simplistic equations such as:

$$D_{eff} = D_{bulk} \frac{\varepsilon}{\tau} \quad (115)$$

Where ε is the catalyst porosity and τ stands for tortuosity. Nevertheless, Eq. 115 is not recommended in solid-liquid systems, and other approaches are suggested such as the one proposed by Ternan (Sievers et al., 2016).

To avoid the determination of D_{eff} (which is not trivial), other strategies have been adopted. Hence, the Madon−Boudart Test based on the work of Koros−Nowak Criterion does not necessitate the calculation of D_{eff}. Application of this criteria only requires the accomplishment of experiments carried out varying the number of active sites.

Once mass transport limitations are ruled out, the rate of RH elimination will show different forms depending on the mechanism taken place at the catalyst surface and the rate limiting step (adsorption, desorption or surface reaction) governing the kinetics of the process. Hence, if PMS must be adsorbed onto the catalyst surface and further activated to generate radicals or any other reactive species, the following reaction should be considered:

$$HSO_5^- + [Cat_{ActiveSite}] \rightleftarrows [HSO_5^- \mapsto [Cat_{ActiveSite}]] \quad K_{eq1} = k_{ads}/k_{des} \quad (116)$$

If adsorption of RH is also required (at similar active sites):

$$RH + [Cat_{ActiveSite}] \rightleftarrows [RH \mapsto [Cat_{ActiveSite}]] \quad K_{eq2} = k_{ads}/k_{des} \quad (117)$$

Now, if only PMS decomposes at the catalyst surface

$$[HSO_5^- \mapsto [Cat_{ActiveSite}]] \rightarrow \begin{cases} SO_4^{-\bullet} \\ HO^{\bullet} \end{cases} + [Cat_{ActiveSite}] + (H_2O, SO_4^{=}, .) \quad k_s \quad (118)$$

The rate of PMS decomposition and radical formation should be:

$$-\frac{dC_{HSO_5^-}}{dt} = \frac{k_s K_{eq1} C_{[Cat_{ActiveSite}]_o} C_{HSO_5^-}}{1 + \frac{k_s}{k_{des}} + K_{eq1} C_{HSO_5^-}} = \frac{k_\alpha C_{[Cat_{ActiveSite}]_o} C_{HSO_5^-}}{1 + k_\beta C_{HSO_5^-}} \quad (119)$$

Expression 119 is the well-known Langmuir Hinselwood kinetics, derived assuming the surface reaction (reaction 118) as the limiting rate. If the surface reaction involves the adsorbed species PMS and RH:

$$[HSO_5^- \mapsto [Cat_{ActiveSite}]] + [RH \mapsto [Cat_{ActiveSite}]] \rightarrow Products + 2[Cat_{ActiveSite}] \quad k_s \quad (120)$$

and the surface reaction is the slow stage, the following expression applies:

$$-\frac{dC_{HSO_5^-}}{dt} = \frac{k_s K_{eq1} K_{eq2} C_{[Cat_{ActiveSite}]_o} C_{RH} C_{HSO_5^-}}{\left(1 + K_{eq1} C_{HSO_5^-} + K_{eq2} C_{RH}\right)^2} \quad (121)$$

Other scenarios can also occur, for instance the implication of two PMS molecules at the catalyst surface in an Eley Rideal type reaction:

$$[HSO_5^- \mapsto [Cat_{ActiveSite}]] + HSO_5^- \rightarrow \begin{cases} SO_4^{-\bullet} \\ HO^{\bullet} \end{cases} + [Cat_{ActiveSite}] + (H_2O, SO_4^{=}, .) \quad k_s \quad (122)$$

Which would lead to an expression such as:

$$-\frac{dC_{HSO_5^-}}{dt} = \frac{k_s K_{eq1} C_{[Cat_{ActiveSite}]_o} C_{HSO_5^-}^2}{1 + K_{eq1} C_{HSO_5^-}} \quad (123)$$

Additionally, if the adsorption of reactants or desorption of products are the limiting stages or even, adsorption of RH occurs in active sites different from PMS, other more complicated expression can be obtained.

Obviously one of the simplest cases is derived from expression 119 when $1 << k_\beta C_{HSO_5^-}$, leading to a simple first order rate law for radicals generation. Heterogeneous catalytic decomposition of peroxymonosulfate must be carried out at different conditions to adequately propose a generic expression able to account for different operating circumstances.

No study of parameters influence has been conducted when the initiation stage is accomplished by a catalyst (homogeneous or heterogeneous) as results are expected not to significantly vary from those reported in PMS homogeneous activation.

2.3. Establishment of a generic model

Application to theoretical simulated results: At this point and given the complexity of handling an excessive number of reactions, and unknown affecting parameters, the proposal of a generic model capable of accounting for the influence of main parameters is recommended. Obviously, the model is just based in observations through the reported literature and has no rigorous theoretical background behind. However, as commented previously, simple first order kinetics are commonly used, and in most cases pseudo first order expressions have no wide application over the complete set of operating parameters, nor theory sustaining their use.

The methodology proposes the use of generic power expressions capable of accounting for positive or negative effects of different parameters, even considering the potential Langmuir type behavior of some of them. Hence, the following differential equation is proposed:

$$-\frac{dC_{RH}}{dt} = \left((k_d + k_{ini})\left[1 + \sum_i \frac{k_i^{num} C_i^{\alpha_i}}{1 + k_i^{den} C_i^{\beta_i}}\right]\right) \frac{C_{RH}^{\alpha_{RH}}}{1 + k_{RH} C_{RH}^{\beta_{RH}}} \frac{C_{PMS}^{\alpha_{PMS}}}{1 + k_{PMS} C_{PMS}^{\beta_{PMS}}} \quad (124)$$

Where k_d would account for the direct oxidation of RH by molecular PMS and k_{ini} considers the activation of PMS (by radiation or any other energy-based initiation and homogeneous or heterogeneous catalysis). k_{ini} can be a function of radiation intensity, catalyst load, etc, in these cases, dependency should experimentally be obtained. k_i, α_i and β_i terms in the summation are constants referred to species i (i = chlorides, TOC, carbonates, protons, etc.). Last two terms refer to generic compound RH and PMS.

The methodology should be as follows:

-First, experiments at different initial concentration of RH should be carried out. Hopefully, PMS is in excess, and its concentration should not appreciably change with time. Under this scenario, Eq. 124 reduces to:

$$-\frac{dC_{RH}}{dt} = k_{adjust} \frac{C_{RH}^{\alpha_{RH}}}{1 + k_{RH} C_{RH}^{\beta_{RH}}} \quad (125)$$

$$k_{adjust} = \left((k_d + k_{ini})\left[1 + \sum_i \frac{k_i^{num} C_i^{\alpha_i}}{1 + k_i^{den} C_i^{\beta_i}}\right]\right) \frac{C_{PMS}^{\alpha_{PMS}}}{1 + k_{PMS} C_{PMS}^{\beta_{PMS}}} = k_{var} \frac{C_{PMS}^{\alpha_{PMS}}}{1 + k_{PMS} C_{PMS}^{\beta_{PMS}}} \quad (126)$$

Experiments completed varying the initial load of RH should allow for the determination of k_{adjust}, k_{RH}, α_{RH} and β_{RH}. The number of parameters to be adjusted is 4 and, consequently, fitted values of k_{adjust}, k_{RH}, α_{RH} and β_{RH} that adequately simulates C_{RHo} influence are not unique. As an example, Fig. 11A shows the results obtained by means of Eq. 125 after numerical integration with Euler's method. Estimated parameters used in the simulation were: $k_{adjust} = 5\times10^{-4}$ $M^{1-\alpha RH}$ s^{-1}, $k_{RH} = 6\times10^{3}$ $M^{-\beta RH}$, $\alpha_{RH} = 0.9$ and $\beta_{RH} = 0.52$. Curves correspond to RH initial values of 0.5, 1.0, 2.5 and 5.0×10^{-7} M. The fitting process was applied to data shown in Fig. 3 A.

In this case, the generic model has been applied to results shown in this work, however, can be utilized with any set of data showing smooth depletion profiles. Hence, pure first order should be obtained by assuming $k_{RH} = 0$ and $\alpha_{RH} = 1.0$, while a changing reaction order depending on RH concentration can be obtained, varying from first order ($1 >> k_{RH}C_{RH}^{\beta_{RH}}$) to α_{RH} - β_{RH} if ($1 << k_{RH}C_{RH}^{\beta_{RH}}$).

-Next stage should investigate the role played by PMS. Typically, $C_{PMSo} >> C_{RHo}$ and peroxymonosulfate concentration remains almost constant during the process. If PMS concentration does significantly decrease, a mathematical expression of PMS abatement should be incorporated into Eq. 124 , similarly to Oh et al. (2015). However, considering the most probable scenario (i.e. C_{PMS} constant), Eq. 125 still holds and different values of k_{adjust} should be obtained. The nonlinear fitting of k_{adjust} and C_{PMS} would facilitate the calculation of k_{var}, k_{PMS}, α_{PMS} and β_{PMS}. Again, the model was applied to theoretical results

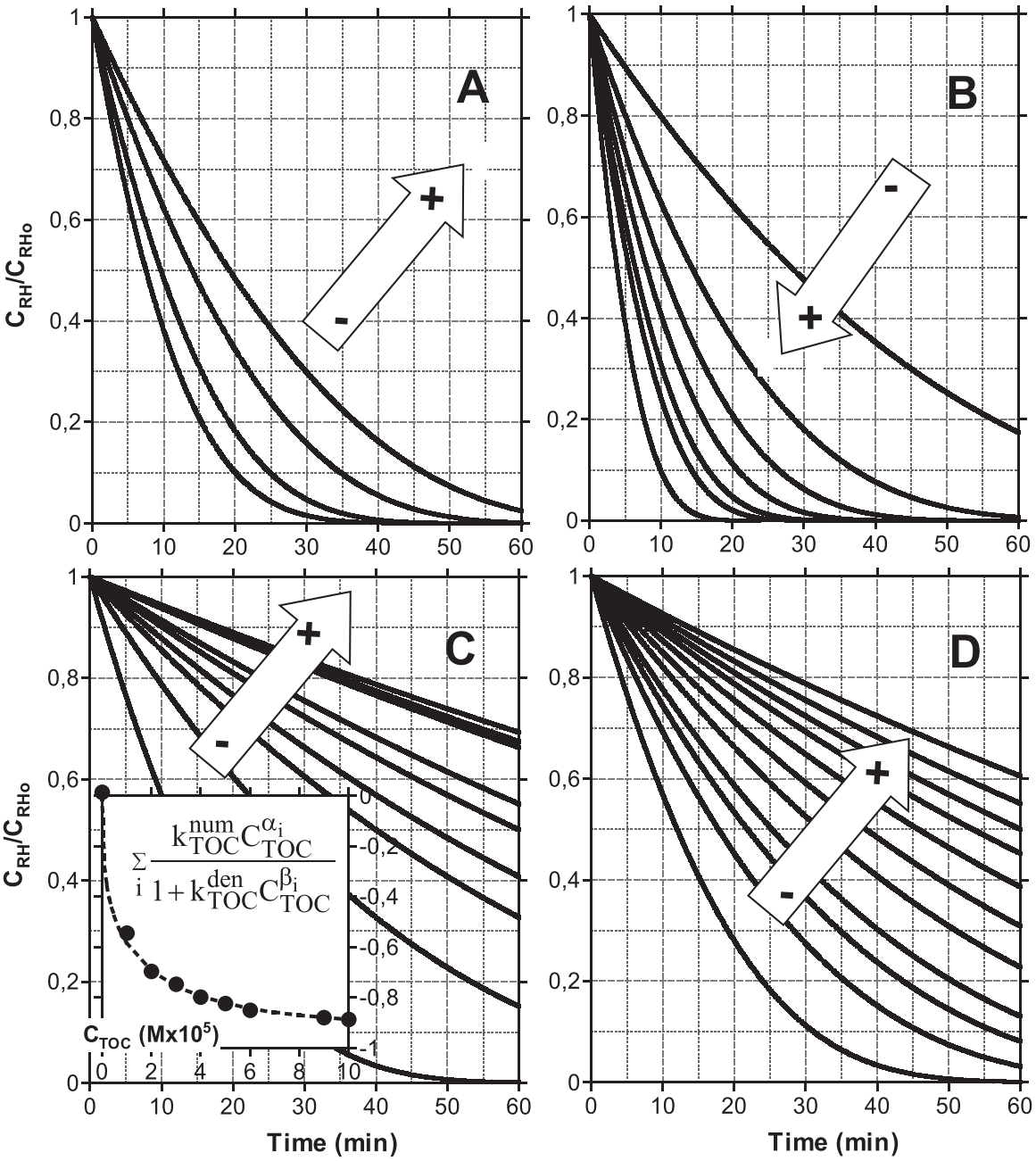

Fig. 11. Simulated removal of the generic compound RH by PMS activation under UV-C radiation. Evolution of RH concentration with time. Generic model application. A- Influence of initial RH concentration from 5.0×10^{-8} to 5.0×10^{-7} M; B- Influence of initial PMS concentration from 35.0×10^{-5} to 5.0×10^{-4} M. C- Influence of initial TOC concentration from 0 to 1.0×10^{-4} M (inset evolution of $\frac{k_{TOC}^{num} C_{TOCo}^{\alpha_i}}{1+k_{TOC}^{den} C_{TOCo}^{\beta_i}}$ versus C_{TOCo}). D- Influence of initial chlorides concentration from 0 to 4.0×10^{-5} M at pH 3. General conditions: $C_{PMSo} = 1\times10^{-4}$ M, $C_{RHo} = 1\times10^{-7}$ M, pH = 7.

obtained by the detailed mechanism shown in Fig. 3B. Modelling of RH profiles was accomplished by changing the PMS concentration used with values of 3.0, 8.22, 13.4, 18.7, 23.9, 29.1 and 50.0×10^{-5} M, obtaining values of k_{adjust} of 1.7, 3.35, 4.7, 6.0, 7.5, 8.7 and 12.5×10^{-4} $M^{1-\alpha RH}$ s^{-1}, respectively (initial RH concentration = 10^{-7} M). Since no negative effect of PMS concentration was obtained, Eq. 126 could be reduced to $k_{adjust} = 0.291 \times C_{PMS_o}^{0.717}$.

-Finally, the influence of other parameters should be faced with a similar strategy. For instance, if TOC shows a negative effect (as assumed in Fig. 5), experiments conducted at different concentrations of TOC would facilitate the determination of its influence. Hence, after considering the information obtained in previous stages, the generic model was applied to experiments simulated by PMS/UV activation in the absence of other influencing parameters apart of TOC. Accordingly, the observed RH abatement as a function of initial TOC should follow the expression:

$$-\frac{dC_{RH}}{dt} = \left((k_d + k_{ini})\left[1 + \frac{k_{TOC}^{num} C_{TOC_o}^{\alpha_i}}{1 + k_{TOC}^{den} C_{TOC_o}^{\beta_i}}\right]\right) \frac{C_{RH}^{0.9}}{1 + 6\times10^3 C_{RH}^{0.52}} C_{PMS_o}^{0.717} \quad (127)$$

From Eq. 127 , in the absence of TOC and $C_{PMS} = 10^{-4}$ M, the term $(k_d+k_{ini}) = 0.291$. Experiments completed with initial TOC concentration from 0 to 10^{-4} M led to values of $\frac{k_{TOC}^{num} C_{TOC_o}^{\alpha_i}}{1+k_{TOC}^{den} C_{TOC_o}^{\beta_i}}$ shown in the inset of Fig. 11C as a function of TOC initial load, generating the expression $\frac{-45\times C_{TOC_o}^{0.364}}{1+400\times C_{TOC_o}^{0.679}}$. Fig. 11C depicts the influence of initial TOC after introducing the Langmuir type equation obtained.

Analogously, the effect of chlorides should be considered with a similar approach. Hence, Fig. 11D shows the influence of increasing concentrations of chlorides from 0 to 4.0×10^{-4} M according to Eq. 128 ($C_{PMSo} = 10^{-4}$ M, $C_{RHo} = 10^{-7}$ M). The fitting process was conducted by considering data shown in Fig. 6A:

$$-\frac{dC_{RH}}{dt} = \left((k_d + k_{ini})\left[1 + \frac{-42.5\times C_{Cl_o^-}^{0.47}}{1 + 50.0\times C_{Cl_o^-}^{0.679}}\right]\right) \frac{C_{RH}^{0.9}}{1 + 6\times10^3 C_{RH}^{0.52}} C_{PMS_o}^{0.717} \quad (128)$$

In cases where a certain parameter could exert both a negative or positive influence on RH removal rate depending on the concentration, the Langmuir type term corresponding to the specific parameter should be transformed to an expression capable to account for this double effect. A parabolic expression could be an acceptable choice:

$$\frac{aC_{i_o}^2 + bC_{i_o} + c}{1 + k_i^{den} C_{i_o}^{\beta_i}} \quad (129)$$

As an example, Fig. 12 shows the simulation of RH removal in the presence of a generic species "i" which negatively influences RH abatement rate from 0 to 3×10^{-4} M and positively affects RH elimination for concentrations above this value. In Fig. 12 values of 2.5×10^7 $M^{-1}s^{-1}$, − 7600 s^{-1}, and − 0.1 Ms^{-1} were used for the coefficients a, b, and c, respectively. k_{den} and β were given values of 50 $M^{-\beta}$ and 0.679.

3. Conclusions

From the theoretical study presented it can be concluded that the use of a detailed mechanism of elemental reactions is not always a warranty of success in modelling processes. Besides of the increasing mathematical complexity as the number of reactions raises, some of the elemental reactions and/or species commonly included in this type of studies play a negligible role. Additionally, the reactivity of the specific target compounds towards some secondary generated radicals (carbonate, ClDOx, organic radicals, etc.) may affect the process in the opposite direction to the one expected. Modelling of PMS based processes must be carried out after experimental data acquisition. Use of pseudo first order kinetics is a common practice that not always contribute to useful information of the process and influencing parameter effects. Moreover, in most of cases, experimental data are incoherent with the features of

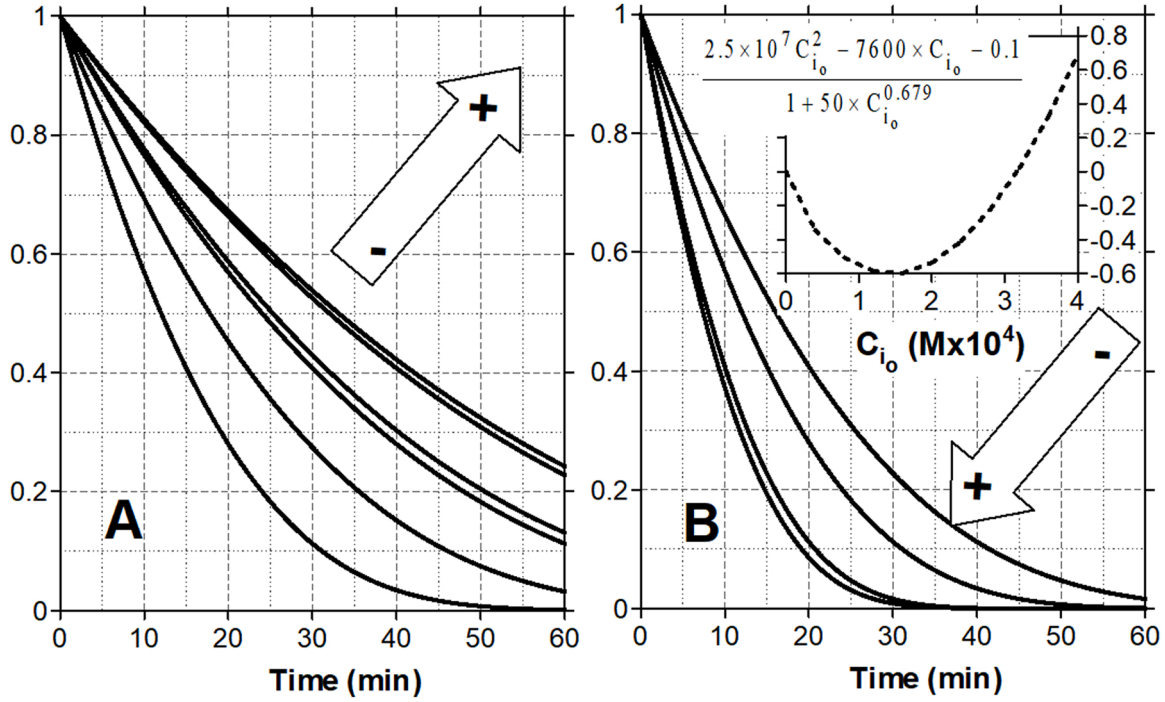

Fig. 12. Simulated removal of the generic compound RH by PMS activation under UV-C radiation. Evolution of RH concentration with time. Generic model application. Influence of initial concentration of influencing parameter "i". A- From 0–3.0×10^{-4} M; B-From 3.0×10^{-4} to 4.0×10^{-4} M. (inset evolution of $\frac{aC_{i_o}^2+bC_{i_o}+c}{1+k_i^{den}C_{i_o}^{\beta_i}}$ versus C_{io}). General conditions: $C_{PMSo} = 1\times10^{-4}$ M, $C_{RHo} = 1\times10^{-7}$ M, pH = 7.

pseudo first order kinetics. From a practical point of view, a model should take into account the influence of main operating variables even with no theoretical background behind. Accordingly, facing the modelling of PMS based processes (and perhaps other advanced oxidation processes) should be attempted either by a mechanism of influencing elemental reactions (neglecting insignificant stages/species) or, alternatively, by a mathematical expression based on empirical results.

Declaration of Competing Interest

The author declares that he has no known competing financial interests or personal relationships that could have appeared to influence the work reported in this paper.

References

Abdul, L., Si, X., Sun, K., Si, Y., 2021. Degradation of bisphenol A in aqueous environment using peroxymonosulfate activated with carbonate: performance, possible pathway, and mechanism. J. Environ. Chem. Eng. 9, 105419 https://doi.org/10.1016/j.jece.2021.105419.

Ahmadi, M., Ghanbari, F., 2018. Combination of UVC-LEDs and ultrasound for peroxymonosulfate activation to degrade synthetic dye: influence of promotional and inhibitory agents and application for real wastewater. Environ. Sci. Pollut. Res. 25, 6003–6014. https://doi.org/10.1007/s11356-017-0936-8.

Anipsitakis, G.P., Dionysiou, D.D., 2004. Radical generation by the interaction of transition metals with common oxidants. Environ. Sci. Technol. 38, 3705–3712. https://doi.org/10.1021/es035121o.

Antonopoulou, M., Kosma, C., Albanis, T., Konstantinou, I., 2021. An overview of homogeneous and heterogeneous photocatalysis applications for the removal of pharmaceutical compounds from real or synthetic hospital wastewaters under lab or pilot scale. Sci. Total Environ. 765, 144163 https://doi.org/10.1016/j.scitotenv.2020.144163.

Ao, X., Liu, W., 2017. Degradation of sulfamethoxazole by medium pressure UV and oxidants: peroxymonosulfate, persulfate, and hydrogen peroxide. Chem. Eng. J. 313, 629–637. https://doi.org/10.1016/j.cej.2016.12.089.

Asadzadeh, S.N., Malakootian, M., Mehdipoor, M., Neyestanaki, D.K., 2021. The removal of tetracycline with biogenic CeO2 nanoparticles in combination with US/PMS process from aqueous solutions: kinetics and mechanism. Water Sci. Technol. 83, 1470–1482. https://doi.org/10.2166/wst.2021.056.

Ashraf, A., Liu, G., Yousaf, B., Arif, M., Ahmed, R., Irshad, S., Cheema, A.I., Rashid, A., Gulzaman, H., 2021. Recent trends in advanced oxidation process-based degradation of erythromycin: pollution status, eco-toxicity and degradation mechanism in aquatic ecosystems. Sci. Total Environ. 772, 145389 https://doi.org/10.1016/j.scitotenv.2021.145389.

Ayol, A., Demiral, Y.O., Gunes, S., 2021. Efficient treatment of domestic wastewaters by using a dynamic membrane bioreactor system. J. Membr. Sci. Res 7, 55–58. https://doi.org/10.22079/jmsr.2020.120244.1330.

Berger, R.J., Stitt, E.H., Marin, G.B., Kapteijn, F., Moulijn, J.A., 2001. Eurokin. Chemical Reaction Kinetics in Practice. CATTECH, pp. 36–60. https://doi.org/10.1023/A:1011928218694.

Berruti, I., Oller, I., Polo-López, M.I., 2021. Direct oxidation of peroxymonosulfate under natural solar radiation: accelerating the simultaneous removal of organic contaminants and pathogens from water. Chemosphere 279, 130555. https://doi.org/10.1016/j.chemosphere.2021.130555.

Bhat, A.P., Gogate, P.R., 2021. Degradation of nitrogen-containing hazardous compounds using advanced oxidation processes: a review on aliphatic and aromatic amines, dyes, and pesticides. J. Hazard. Mater. 403, 123657 https://doi.org/10.1016/j.jhazmat.2020.123657.

Bolton, J.R., Bircher, K.G., Tumas, W., Tolman, C.A., 2001. Figures-of-merit for the technical development and application of advanced oxidation technologies for both electric- and solar-driven systems (IUPAC Technical Report). Pure Appl. Chem. 73, 627–637. https://doi.org/10.1351/pac200173040627.

Canonica, S., Schönenberger, U., 2019. Inhibitory effect of dissolved organic matter on the transformation of selected anilines and sulfonamide antibiotics induced by the sulfate radical. Environ. Sci. Technol. 53, 11783–11791. https://doi.org/10.1021/acs.est.9b04105.

Cederbaum, A.I., Qureshi, A., Cohen, G., 1983. Production of formaldehyde and acetone by hydroxyl-radical generating systems during the metabolism of tertiary butyl alcohol. Biochem. Pharmacol. 32, 3517–3524. https://doi.org/10.1016/0006-2952(83)90297-6.

Chauhan, R., Dinesh, G.K., Alawa, B., Chakma, S., 2021. A critical analysis of sono-hybrid advanced oxidation process of ferrioxalate system for degradation of recalcitrant pollutants. Chemosphere 277, 130324. https://doi.org/10.1016/j.chemosphere.2021.130324.

Chen, D., Ma, X., Zhou, J., Chen, X., Qian, G., 2014. Sulfate radical-induced degradation of Acid Orange 7 by a new magnetic composite catalyzed peroxymonosulfate oxidation process. J. Hazard. Mater. 279, 476–484. https://doi.org/10.1016/j.jhazmat.2014.06.004.

Chen, M., Zhu, L., Liu, S., Li, R., Wang, N., Tang, H., 2019. Efficient degradation of organic pollutants by low-level Co2+ catalyzed homogeneous activation of peroxymonosulfate. J. Hazard. Mater. 371, 456–462. https://doi.org/10.1016/j.jhazmat.2019.03.002.

Chen, R., Pignatello, J.J., 1997. Role of quinone intermediates as electron shuttles in fenton and photoassisted fenton oxidations of aromatic compounds. Environ. Sci. Technol. 31, 2399–2406. https://doi.org/10.1021/es9610646.

Chen, X., Qiao, X., Wang, D., Lin, J., Chen, J., 2007. Kinetics of oxidative decolorization and mineralization of Acid Orange 7 by dark and photoassisted Co2+-catalyzed peroxymonosulfate system. Chemosphere 67, 802–808. https://doi.org/10.1016/j.chemosphere.2006.10.032.

Cheng, N., Wang, B., Wu, P., Lee, X., Xing, Y., Chen, M., Gao, B., 2021. Adsorption of emerging contaminants from water and wastewater by modified biochar: a review. Environ. Pollut. 273, 116448 https://doi.org/10.1016/j.envpol.2021.116448.

Chu, Z., Chen, T., Liu, H., Chen, D., Zou, X., Wang, H., Sun, F., Zhai, P., Xia, M., Liu, M., 2021. Degradation of norfloxacin by calcite activating peroxymonosulfate: performance and mechanism. Chemosphere 282, 131091. https://doi.org/10.1016/j.chemosphere.2021.131091.

Davididou, K., Frontistis, Z., 2021. Advanced oxidation processes for the treatment of winery wastewater: a review and future perspectives. J. Chem. Technol. Biotechnol. https://doi.org/10.1002/jctb.6772.

Dinh, M., Hakimabadi, S.G., Pham, A.L.-T., 2020. Treatment of sulfolane in groundwater: a critical review. J. Environ. Manag. 263, 110385 https://doi.org/10.1016/j.jenvman.2020.110385.

Divyapriya, G., Singh, S., Martínez-Huitle, C.A., Scaria, J., Karim, A.V., Nidheesh, P.V., 2021. Treatment of real wastewater by photoelectrochemical methods: an overview. Chemosphere 276, 130188. https://doi.org/10.1016/j.chemosphere.2021.130188.

Djaballah, M.L., Merouani, S., Bendjama, H., Hamdaoui, O., 2021. Development of a free radical-based kinetics model for the oxidative degradation of chlorazol black in aqueous solution using periodate photoactivated process. J. Photochem. Photobiol. A Chem. 408, 113102 https://doi.org/10.1016/j.jphotochem.2020.113102.

Domingues, E., Fernandes, E., Gomes, J., Martins, R.C., 2021. Advanced oxidation processes perspective regarding swine wastewater treatment. Sci. Total Environ. 776, 145958 https://doi.org/10.1016/j.scitotenv.2021.145958.

Dong, H., Xu, Q., Lian, L., Li, Y., Wang, S., Li, C., Guan, X., 2021. Degradation of organic contaminants in the Fe(II)/peroxymonosulfate process under acidic conditions: the overlooked rapid oxidation stage. Environ. Sci. Technol. 55, 15390–15399. https://doi.org/10.1021/acs.est.1c04563.

Duan, P., Liu, X., Liu, B., Akram, M., Li, Y., Pan, J., Yue, Q., Gao, B., Xu, X., 2021. Effect of phosphate on peroxymonosulfate activation: accelerating generation of sulfate radical and underlying mechanism. Appl. Catal. B Environ. 298, 120532 https://doi.org/10.1016/j.apcatb.2021.120532.

Figueredo, M., Rodríguez, E.M., Rivas, J., Beltrán, F.J., 2020. Kinetic model basis of ozone/light-based advanced oxidation processes: a pseudoempirical approach. Environ. Sci. Water Res. Technol. 6, 1176–1185. https://doi.org/10.1039/D0EW00064G.

Fortnum, D.H., Battaglia, C.J., Cohen, S.R., Edwards, J.O., 1960. The kinetics of the oxidation of halide ions by monosubstituted peroxides. J. Am. Chem. Soc. 82, 778–782. https://doi.org/10.1021/ja01489a004.

Gao, P., Tian, X., Fu, W., Wang, Y., Nie, Y., Yang, C., Deng, Y., 2021. Copper in LaMnO3 to promote peroxymonosulfate activation by regulating the reactive oxygen species in sulfamethoxazole degradation. J. Hazard. Mater. 411, 125163 https://doi.org/10.1016/j.jhazmat.2021.125163.

Ghanbari, F., Moradi, M., 2017. Application of peroxymonosulfate and its activation methods for degradation of environmental organic pollutants: review. Chem. Eng. J. 310, 41–62. https://doi.org/10.1016/j.cej.2016.10.064.

Giannakis, S., Lin, K.-Y.A., Ghanbari, F., 2021. A review of the recent advances on the treatment of industrial wastewaters by Sulfate Radical-based Advanced Oxidation Processes (SR-AOPs). Chem. Eng. J. 406, 127083 https://doi.org/10.1016/j.cej.2020.127083.

Gimeno, O., Rivas, J., Carbajo, M., Borralho, T., 2009. Catalytic decomposition of potassium monopersulfate. Kinetics. https://doi.org/10.5281/ZENODO.1055661.

Golshan, M., Kakavandi, B., Ahmadi, M., Azizi, M., 2018. Photocatalytic activation of peroxymonosulfate by TiO2 anchored on cupper ferrite (TiO2@CuFe2O4) into 2,4-D degradation: process feasibility, mechanism and pathway. J. Hazard. Mater. 359, 325–337. https://doi.org/10.1016/j.jhazmat.2018.06.069.

Gong, Han, Chu, W., Xu, K., Xia, X., Gong, He, Tan, Y., Pu, S., 2020. Efficient degradation, mineralization and toxicity reduction of sulfamethoxazole under photo-activation of peroxymonosulfate by ferrate (VI). Chem. Eng. J. 389, 124084 https://doi.org/10.1016/j.cej.2020.124084.

Guan, Y.-H., Ma, J., Li, X.-C., Fang, J.-Y., Chen, L.-W., 2011. Influence of pH on the formation of sulfate and hydroxyl radicals in the UV/peroxymonosulfate system. Environ. Sci. Technol. 45, 9308–9314. https://doi.org/10.1021/es2017363.

Guerra-Rodríguez, S., Ribeiro, A.R.L., Ribeiro, R.S., Rodríguez, E., Silva, A.M.T., Rodríguez-Chueca, J., 2021. UV-A activation of peroxymonosulfate for the removal of micropollutants from secondary treated wastewater. Sci. Total Environ. 770, 145299 https://doi.org/10.1016/j.scitotenv.2021.145299.

Guerreiro, R.C.S., Jerónimo, E., Luz, S., Pinheiro, H.M., Prazeres, A.R., 2020. Cheese manufacturing wastewater treatment by combined physicochemical processes for reuse and fertilizer production. J. Environ. Manag. 264, 110470 https://doi.org/10.1016/j.jenvman.2020.110470.

Guo, C., Chen, C., Lu, J., Fu, D., Yuan, C.-Z., Wu, X.-L., Hui, K.N., Chen, J., 2021. Stable and recyclable Fe3C@CN catalyst supported on carbon felt for efficient activation of peroxymonosulfate. J. Colloid Interface Sci. 599, 219–226. https://doi.org/10.1016/j.jcis.2021.04.092.

Guo, Y., Yan, L., Li, X., Yan, T., Song, W., Hou, T., Tong, C., Mu, J., Xu, M., 2021. Goethite/biochar-activated peroxymonosulfate enhances tetracycline degradation:

inherent roles of radical and non-radical processes. Sci. Total Environ. 783, 147102 https://doi.org/10.1016/j.scitotenv.2021.147102.
Guyu, S., Kee, O.S., 2022. Oxidation of 2,4-dichlorophenoxyacetic acid by persulfate or peroxymonosulfate with iron(II) as an activator. J. Hazard. Toxic., Radioact. Waste 26, 4021036. https://doi.org/10.1061/(ASCE)HZ.2153-5515.0000645.
He, J., Xie, T., Luo, T., Xu, Q., Ye, F., An, J., Yang, J., Wang, J., 2021. Enhanced peroxymonosulfate activation over heterogeneous catalyst Cu0.76Co2.24O4/SBA-15 for efficient degradation of sulfapyridine antibiotic. Ecotoxicol. Environ. Saf. 216, 112189 https://doi.org/10.1016/j.ecoenv.2021.112189.
Henze, M., van Loosdrecht, M.C.M., Ekama, G.A., Brdjanovic, D., 2008. Biological Wastewater Treatment: Principles, Modeling and Design. IWA Publishing. https://doi.org/10.2166/9781780401867.
Herrmann, H., Ervens, B., Jacobi, H.-W., Wolke, R., Nowacki, P., Zellner, R., 2000. CAPRAM2.3: a chemical aqueous phase radical mechanism for tropospheric chemistry. J. Atmos. Chem. 36, 231–284. https://doi.org/10.1023/A:1006318622743.
Hong, Q., Liu, C., Wang, Z., Li, R., Liang, X., Wang, Y., Zhang, Y., Song, Z., Xiao, Z., Cui, T., Heng, B., Xu, B., Qi, F., Ikhlaq, A., 2021. Electron transfer enhancing Fe(II)/Fe(III) cycle by sulfur and biochar in magnetic FeS@biochar to active peroxymonosulfate for 2,4-dichlorophenoxyacetic acid degradation. Chem. Eng. J. 417, 129238 https://doi.org/10.1016/j.cej.2021.129238.
Hoops, S., Sahle, S., Gauges, R., Lee, C., Pahle, J., Simus, N., Singhal, M., Xu, L., Mendes, P., Kummer, U., 2006. COPASI—a complex pathway simulator. Bioinformatics 22, 3067–3074. https://doi.org/10.1093/bioinformatics/btl485.
Hou, J., He, X., Zhang, S., Yu, J., Feng, M., Li, X., 2021. Recent advances in cobalt-activated sulfate radical-based advanced oxidation processes for water remediation: a review. Sci. Total Environ. 770, 145311 https://doi.org/10.1016/j.scitotenv.2021.145311.
Hu, J., Chen, H., Dong, H., Zhu, L., Qiang, Z., Yu, J., 2021. Transformation of iopamidol and atrazine by peroxymonosulfate under catalysis of a composite iron corrosion product (Fe/Fe3O4): electron transfer, active species and reaction pathways. J. Hazard. Mater. 403, 123553 https://doi.org/10.1016/j.jhazmat.2020.123553.
Hu, J., Zhang, J., Wang, Q., Ye, Q., Xu, H., Zhou, G., Lu, J., 2019. Efficient degradation of tetracycline by ultraviolet-based activation of peroxymonosulfate and persulfate. Water Sci. Technol. 79, 911–920. https://doi.org/10.2166/wst.2019.034.
Hu, P., Long, M., 2016. Cobalt-catalyzed sulfate radical-based advanced oxidation: a review on heterogeneous catalysts and applications. Appl. Catal. B Environ. 181, 103–117. https://doi.org/10.1016/j.apcatb.2015.07.024.
Huang, Y.-H., Huang, Y.-F., Huang, C., Chen, C.-Y., 2009. Efficient decolorization of azo dye Reactive Black B involving aromatic fragment degradation in buffered Co2+/PMS oxidative processes with a ppb level dosage of Co2+-catalyst. J. Hazard. Mater. 170, 1110–1118. https://doi.org/10.1016/j.jhazmat.2009.05.091.
Huang, Y., Li, X., Zhang, C., Dai, M., Zhang, Z., Xi, Y., Quan, B., Lu, S., Liu, Y., 2021. Degrading arsanilic acid and adsorbing the released inorganic arsenic simultaneously in aqueous media with CuFe2O4 activating peroxymonosulfate system: factors, performance, and mechanism. Chem. Eng. J. 424, 128537 https://doi.org/10.1016/j.cej.2021.128537.
Huang, Z., Wu, P., Liu, C., Chen, M., Yang, S., Dang, Z., Zhu, N., 2021. Multiple catalytic reaction sites induced non-radical/radical pathway with graphene layers encapsulated Fe-N-C toward highly efficient peroxymonosulfate (PMS) activation. Chem. Eng. J. 413, 127507 https://doi.org/10.1016/j.cej.2020.127507.
Ike, I.A., Linden, K.G., Orbell, J.D., Duke, M., 2018. Critical review of the science and sustainability of persulphate advanced oxidation processes. Chem. Eng. J. 338, 651–669. https://doi.org/10.1016/j.cej.2018.01.034.
Javaid, R., Qazi, U.Y., Ikhlaq, A., Zahid, M., Alazmi, A., 2021. Subcritical and supercritical water oxidation for dye decomposition. J. Environ. Manag. 290, 112605 https://doi.org/10.1016/j.jenvman.2021.112605.
Jørgensen, S.E.B.T.-S., 1979. Chapter 3 precipitation, coagulation and flocculation. In: E. S. (Ed.), Industrial Waste Water Management. Elsevier, pp. 25–37. https://doi.org/10.1016/S0166-1116(08)71594-2.
Kanjal, M.I., Muneer, M., Abdelhaleem, A., Chu, W., 2020. Degradation of methotrexate by UV/peroxymonosulfate: kinetics, effect of operational parameters and mechanism. Chin. J. Chem. Eng. 28, 2658–2667. https://doi.org/10.1016/j.cjche.2020.05.033.
Kim, J., Edwards, J.O., 1995. A study of cobalt catalysis and copper modification in the coupled decompositions of hydrogen peroxide and peroxomonosulfate ion. Inorg. Chim. Acta 235, 9–13. https://doi.org/10.1016/0020-1693(95)90039-9.
Ko, C.-H., Hsieh, P.-H., Chang, M.-W., Chern, J.-M., Chiang, S.-M., Tzeng, C.-J., 2009. Kinetics of pulp mill effluent treatment by ozone-based processes. J. Hazard. Mater. 168, 875–881. https://doi.org/10.1016/j.jhazmat.2009.02.111.
Korpe, S., Rao, P.V., 2021. Application of advanced oxidation processes and cavitation techniques for treatment of tannery wastewater—a review. J. Environ. Chem. Eng. 9, 105234 https://doi.org/10.1016/j.jece.2021.105234.
Lal, K., Garg, A., 2017. Physico-chemical treatment of pulping effluent: characterization of flocs and sludge generated after treatment. Sep. Sci. Technol. 52, 1583–1593. https://doi.org/10.1080/01496395.2017.1292294.
Lee, J., von Gunten, U., Kim, J.-H., 2020. Persulfate-based advanced oxidation: critical assessment of opportunities and roadblocks. Environ. Sci. Technol. 54, 3064–3081. https://doi.org/10.1021/acs.est.9b07082.
Lei, Y., Cheng, S., Luo, N., Yang, X., An, T., 2019. Rate constants and mechanisms of the reactions of Cl•• and Cl2•– with trace organic contaminants. Environ. Sci. Technol. 53, 11170–11182. https://doi.org/10.1021/acs.est.9b02462.
Li, Huanxuan, Yang, Z., Lu, S., Su, L., Wang, C., Huang, J., Zhou, J., Tang, J., Huang, M., 2021a. Nano-porous bimetallic CuCo-MOF-74 with coordinatively unsaturated metal sites for peroxymonosulfate activation to eliminate organic pollutants: Performance and mechanism. Chemosphere 273, 129643. https://doi.org/10.1016/j.chemosphere.2021.129643.
Li, Huanxuan, Yao, Y., Chen, J., Wang, C., Huang, J., Du, J., Xu, S., Tang, J., Zhao, H., Huang, M., 2021b. Heterogeneous activation of peroxymonosulfate by bimetallic MOFs for efficient degradation of phenanthrene: synthesis, performance, kinetics, and mechanisms. Sep. Purif. Technol. 259, 118217 https://doi.org/10.1016/j.seppur.2020.118217.
Li, Hongchao, Zhao, Z., Qian, J., Pan, B., 2021. Are free radicals the primary reactive species in Co(II)-mediated activation of peroxymonosulfate? new evidence for the role of the Co(II)–peroxymonosulfate complex. Environ. Sci. Technol. 55, 6397–6406. https://doi.org/10.1021/acs.est.1c02015.
Li, N., Lu, X., He, M., Duan, X., Yan, B., Chen, G., Wang, S., 2021. Catalytic membrane-based oxidation-filtration systems for organic wastewater purification: a review. J. Hazard. Mater. 414, 125478 https://doi.org/10.1016/j.jhazmat.2021.125478.
Li, Y., Yang, Y., Lei, J., Liu, W., Tong, M., Liang, J., 2021. The degradation pathways of carbamazepine in advanced oxidation process: a mini review coupled with DFT calculation. Sci. Total Environ. 779, 146498 https://doi.org/10.1016/j.scitotenv.2021.146498.
Liang, J., Fu, L., 2021. Activation of peroxymonosulfate (PMS) by Co3O4 quantum dots decorated hierarchical C@Co3O4 for degradation of organic pollutants: kinetics and radical-nonradical cooperation mechanisms. Appl. Surf. Sci. 563, 150335 https://doi.org/10.1016/j.apsusc.2021.150335.
Lin, Z., Qin, W., Sun, L., Yuan, X., Xia, D., 2020. Kinetics and mechanism of sulfate radical- and hydroxyl radical-induced degradation of Bisphenol A in VUV/UV/peroxymonosulfate system. J. Water Process Eng. 38, 101636 https://doi.org/10.1016/j.jwpe.2020.101636.
Ling, S.K., Wang, S., Peng, Y., 2010. Oxidative degradation of dyes in water using Co2+/H2O2 and Co2+/peroxymonosulfate. J. Hazard. Mater. 178, 385–389. https://doi.org/10.1016/j.jhazmat.2010.01.091.
Liu, K., Bai, L., Shi, Y., Wei, Z., Spinney, R., Göktaş, R.K., Dionysiou, D.D., Xiao, R., 2020. Simultaneous disinfection of E. faecalis and degradation of carbamazepine by sulfate radicals: an experimental and modelling study. Environ. Pollut. 263, 114558 https://doi.org/10.1016/j.envpol.2020.114558.
Liu, S., Zhang, Z., Huang, F., Liu, Y., Feng, L., Jiang, J., Zhang, L., Qi, F., Liu, C., 2021. Carbonized polyaniline activated peroxymonosulfate (PMS) for phenol degradation: role of PMS adsorption and singlet oxygen generation. Appl. Catal. B Environ. 286, 119921 https://doi.org/10.1016/j.apcatb.2021.119921.
Luo, C., Ma, J., Jiang, J., Liu, Y., Song, Y., Yang, Y., Guan, Y., Wu, D., 2015. Simulation and comparative study on the oxidation kinetics of atrazine by UV/H2O2, UV/HSO5− and UV/S2O82−. Water Res. 80, 99–108. https://doi.org/10.1016/j.watres.2015.05.019.
Luo, M., Zhou, H., Zhou, P., Lai, L., Liu, W., Ao, Z., Yao, G., Zhang, H., Lai, B., 2021. Insights into the role of in-situ and ex-situ hydrogen peroxide for enhanced ferrate (VI) towards oxidation of organic contaminants. Water Res. 203, 117548 https://doi.org/10.1016/j.watres.2021.117548.
Lutze, H.V., Kerlin, N., Schmidt, T.C., 2015. Sulfate radical-based water treatment in presence of chloride: formation of chlorate, inter-conversion of sulfate radicals into hydroxyl radicals and influence of bicarbonate. Water Res. 72, 349–360. https://doi.org/10.1016/j.watres.2014.10.006.
Ma, D., Yi, H., Lai, C., Liu, X., Huo, X., An, Z., Li, L., Fu, Y., Li, B., Zhang, M., Qin, L., Liu, S., Yang, L., 2021. Critical review of advanced oxidation processes in organic wastewater treatment. Chemosphere 275, 130104. https://doi.org/10.1016/j.chemosphere.2021.130104.
Matthew, B.M., Anastasio, C., 2006. A chemical probe technique for the determination of reactive halogen species in aqueous solution: part 1 – bromide solutions. Atmos. Chem. Phys. 6, 2423–2437. https://doi.org/10.5194/acp-6-2423-2006.
Meng, W., Wang, Y., Zhang, Y., Liu, C., Wang, Z., Song, Z., Xu, B., Qi, F., Ikhlaq, A., 2020. Degradation Rhodamine B dye wastewater by sulfate radical-based visible light-fenton mediated by LaFeO3: reaction mechanism and empirical modeling. J. Taiwan Inst. Chem. Eng. 111, 162–169. https://doi.org/10.1016/j.jtice.2020.04.005.
Merle, T., Pic, J.S., Manero, M.H., Debellefontaine, H., 2009. Enhanced bio-recalcitrant organics removal by combined adsorption and ozonation. Water Sci. Technol. a J. Int. Assoc. Water Pollut. Res 60, 2921–2928. https://doi.org/10.2166/wst.2009.711.
Miklos, D.B., Remy, C., Jekel, M., Linden, K.G., Drewes, J.E., Hübner, U., 2018. Evaluation of advanced oxidation processes for water and wastewater treatment – a critical review. Water Res 139, 118–131. https://doi.org/10.1016/j.watres.2018.03.042.
Milh, H., Cabooter, D., Dewil, R., 2022. Degradation of sulfamethoxazole by ferrous iron activated peroxymonosulfate: elucidation of the degradation mechanism and influence of process parameters. Chem. Eng. J. 430, 132875 https://doi.org/10.1016/j.cej.2021.132875.
Minakata, D., Kamath, D., Maetzold, S., 2017. Mechanistic insight into the reactivity of chlorine-derived radicals in the aqueous-phase UV–chlorine advanced oxidation process: quantum mechanical calculations. Environ. Sci. Technol. 51, 6918–6926. https://doi.org/10.1021/acs.est.7b00507.
Mpatani, F.M., Aryee, A.A., Kani, A.N., Han, R., Li, Z., Dovi, E., Qu, L., 2021. A review of treatment techniques applied for selective removal of emerging pollutant-trimethoprim from aqueous systems. J. Clean. Prod. 308, 127359 https://doi.org/10.1016/j.jclepro.2021.127359.
Nesan, D., Rajantrakumar, N.K., Chan, D.J.C., 2021. Membrane filtration pretreatment and phytoremediation of fish farm wastewater. J. Membr. Sci. Res 7, 38–44. https://doi.org/10.22079/jmsr.2020.120104.1324.
Neta, P., Huie, R.E., Ross, A.B., 1988. Rate constants for reactions of inorganic radicals in aqueous solution. J. Phys. Chem. Ref. Data 17, 1027–1284. https://doi.org/10.1063/1.555808.

Nie, M., Zhang, W., Yan, C., Xu, W., Wu, L., Ye, Y., Hu, Y., Dong, W., 2019. Enhanced removal of organic contaminants in water by the combination of peroxymonosulfate and carbonate. Sci. Total Environ. 647, 734–743. https://doi.org/10.1016/j.scitotenv.2018.08.065.

Oba, S.N., Ighalo, J.O., Aniagor, C.O., Igwegbe, C.A., 2021. Removal of ibuprofen from aqueous media by adsorption: a comprehensive review. Sci. Total Environ. 780, 146608 https://doi.org/10.1016/j.scitotenv.2021.146608.

Oh, W.-D., Dong, Z., Hu, Z.-T., Lim, T.-T., 2015. A novel quasi-cubic CuFe2O4–Fe2O3 catalyst prepared at low temperature for enhanced oxidation of bisphenol A via peroxymonosulfate activation. J. Mater. Chem. A 3, 22208–22217. https://doi.org/10.1039/C5TA06563A.

Oh, W.-D., Dong, Z., Lim, T.-T., 2016. Generation of sulfate radical through heterogeneous catalysis for organic contaminants removal: current development, challenges and prospects. Appl. Catal. B Environ. 194, 169–201. https://doi.org/10.1016/j.apcatb.2016.04.003.

Pantziaros, A.G., Jaho, S., Karga, I., Iakovides, I.C., Koutsoukos, P.G., Paraskeva, C.A., 2018. Struvite precipitation and COD reduction in a two-step treatment of olive mill wastewater. J. Chem. Technol. Biotechnol. 93, 730–735. https://doi.org/10.1002/jctb.5422.

Peng, G., You, W., Zhou, W., Zhou, G., Qi, C., Hu, Y., 2021. Activation of peroxymonosulfate by phosphite: kinetics and mechanism for the removal of organic pollutants. Chemosphere 266, 129016. https://doi.org/10.1016/j.chemosphere.2020.129016.

Peng, J., Wang, Z., Wang, S., Liu, J., Zhang, Y., Wang, B., Gong, Z., Wang, M., Dong, H., Shi, J., Liu, H., Yan, G., Liu, G., Gao, S., Cao, Z., 2021. Enhanced removal of methylparaben mediated by cobalt/carbon nanotubes (Co/CNTs) activated peroxymonosulfate in chloride-containing water: reaction kinetics, mechanisms and pathways. Chem. Eng. J. 409, 128176 https://doi.org/10.1016/j.cej.2020.128176.

Peng, Y., Shi, H., Wang, Z., Fu, Y., Liu, Y., 2021. Kinetics and reaction mechanism of photochemical degradation of diclofenac by UV-activated peroxymonosulfate. RSC Adv. 11, 6804–6817. https://doi.org/10.1039/D0RA10178H.

Pérez-Moya, M., Mansilla, H.D., Graells, M., 2011. A practical parametrical characterization of the Fenton and the photo-Fenton sulfamethazine treatment using semi-empirical modeling. J. Chem. Technol. Biotechnol. 86, 826–831. https://doi.org/10.1002/jctb.2595.

Qi, F., Chu, W., Xu, B., 2013. Catalytic degradation of caffeine in aqueous solutions by cobalt-MCM41 activation of peroxymonosulfate. Appl. Catal. B Environ. 134–135, 324–332. https://doi.org/10.1016/j.apcatb.2013.01.038.

Qi, Y., Qu, R., Liu, J., Chen, J., Al-Basher, G., Alsultan, N., Wang, Z., Huo, Z., 2019. Oxidation of flumequine in aqueous solution by UV-activated peroxymonosulfate: kinetics, water matrix effects, degradation products and reaction pathways. Chemosphere 237, 124484. https://doi.org/10.1016/j.chemosphere.2019.124484.

Rastogi, A., Al-Abed, S.R., Dionysiou, D.D., 2009. Sulfate radical-based ferrous–peroxymonosulfate oxidative system for PCBs degradation in aqueous and sediment systems. Appl. Catal. B Environ. 85, 171–179. https://doi.org/10.1016/j.apcatb.2008.07.010.

Rehman, F., Sayed, M., Khan, J.A., Shah, N.S., Khan, H.M., Dionysiou, D.D., 2018. Oxidative removal of brilliant green by UV/S2O82–, UV/HSO5– and UV/H2O2 processes in aqueous media: a comparative study. J. Hazard. Mater. 357, 506–514. https://doi.org/10.1016/j.jhazmat.2018.06.012.

Ren, M., Drosos, M., Frimmel, F.H., 2018. Inhibitory effect of NOM in photocatalysis process: explanation and resolution. Chem. Eng. J. 334, 968–975. https://doi.org/10.1016/j.cej.2017.10.099.

Rivas, F.J., Beltrán, F.J., Garcia-araya, J.F., Navarrete, V., Gimeno, O., 2002. Co-oxidation of p-hydroxybenzoic acid and atrazine by the Fenton's like system Fe(III)/H2O2. J. Hazard. Mater. 91, 143–157. https://doi.org/10.1016/S0304-3894(01)00381-8.

Rivas, F.J., Beltrán, F.J., Gimeno, O., Alvarez, P., 2003. Treatment of brines by combined Fenton's reagent–aerobic biodegradation: II. Process modelling. J. Hazard. Mater. 96, 259–276. https://doi.org/10.1016/S0304-3894(02)00216-9.

Rivas, F.J., Beltrán, F.J., Gimeno, O., Carbajo, M., 2006. Fluorene oxidation by coupling of ozone, radiation, and semiconductors: a mathematical approach to the kinetics. Ind. Eng. Chem. Res. 45, 166–174. https://doi.org/10.1021/ie050781i.

Rivas, F.J., Frades, J., Alonso, M.A., Montoya, C., Monteagudo, J.M., 2005. Fenton's oxidation of food processing wastewater components. kinetic modeling of protocatechuic acid degradation. J. Agric. Food Chem. 53, 10097–10104. https://doi.org/10.1021/jf0512712.

Rivas, F.J., García, R., García-Araya, J.F., Gimeno, O., 2008. Promoted wet air oxidation of polynuclear aromatic hydrocarbons. J. Hazard. Mater. 153, 792–798. https://doi.org/10.1016/j.jhazmat.2007.09.025.

Rivas, F.J., Gimeno, O., Borallho, T., 2012. Aqueous pharmaceutical compounds removal by potassium monopersulfate. Uncatalyzed and catalyzed semicontinuous experiments. Chem. Eng. J. 192, 326–333. https://doi.org/10.1016/j.cej.2012.03.055.

Rivas, F.J., Kolaczkowski, S.T., Beltrán, F.J., McLurgh, D.B., 1998. Development of a model for the wet air oxidation of phenol based on a free radical mechanism. Chem. Eng. Sci. 53, 2575–2586. https://doi.org/10.1016/S0009-2509(98)00060-8.

Rivas, F.J., Solís, R.R., 2018. Chloride promoted oxidation of tritosulfuron by peroxymonosulfate. Chem. Eng. J. 349, 728–736. https://doi.org/10.1016/j.cej.2018.05.117.

Rivas, J., Solis, R.R., Gimeno, O., Sagasti, J., 2015. Photocatalytic elimination of aqueous 2-methyl-4-chlorophenoxyacetic acid in the presence of commercial and nitrogen-doped TiO2. Int. J. Environ. Sci. Technol. 12, 513–526. https://doi.org/10.1007/s13762-013-0452-4.

Rodríguez-Narvaez, O.M., Rajapaksha, R.D., Ranasinghe, M.I., Bai, X., Peralta-Hernández, J.M., Bandala, E.R., 2020. Peroxymonosulfate decomposition by homogeneous and heterogeneous Co: kinetics and application for the degradation of acetaminophen. J. Environ. Sci. 93, 30–40. https://doi.org/10.1016/j.jes.2020.03.002.

Santiago, E., Sandra, C., O.D, F., 2004. Engineering aspects of the integration of chemical and biological oxidation: simple mechanistic models for the oxidation treatment. J. Environ. Eng. 130, 967–974. https://doi.org/10.1061/(ASCE)0733-9372(2004)130:9(967).

Saravanan, A., Senthil Kumar, P., Jeevanantham, S., Karishma, S., Tajsabreen, B., Yaashikaa, P.R., Reshma, B., 2021. Effective water/wastewater treatment methodologies for toxic pollutants removal: processes and applications towards sustainable development. Chemosphere 280, 130595. https://doi.org/10.1016/j.chemosphere.2021.130595.

Sarria, V., Parra, S., Adler, N., Péringer, P., Benitez, N., Pulgarin, C., 2002. Recent developments in the coupling of photoassisted and aerobic biological processes for the treatment of biorecalcitrant compounds. Catal. Today 76, 301–315. https://doi.org/10.1016/S0920-5861(02)00228-6.

Shad, A., Chen, J., Qu, R., Dar, A.A., Bin-Jumah, M., Allam, A.A., Wang, Z., 2020. Degradation of sulfadimethoxine in phosphate buffer solution by UV alone, UV/PMS and UV/H2O2: kinetics, degradation products, and reaction pathways. Chem. Eng. J. 398, 125357 https://doi.org/10.1016/j.cej.2020.125357.

Shinohara, K., Shida, T., Saito, N., 1962. Radiation decomposition of aqueous azide solution. J. Chem. Phys. 37, 173–177. https://doi.org/10.1063/1.1732947.

Sievers, C., Noda, Y., Qi, L., Albuquerque, E.M., Rioux, R.M., Scott, S.L., 2016. Phenomena affecting catalytic reactions at solid–liquid interfaces. ACS Catal. 6, 8286–8307. https://doi.org/10.1021/acscatal.6b02532.

Sivaranjanee, R., Kumar, P.S., 2021. A review on cleaner approach for effective separation of toxic pollutants from wastewater using carbon Sphere's as adsorbent: preparation, activation and applications. J. Clean. Prod. 291, 125911 https://doi.org/10.1016/j.jclepro.2021.125911.

Solís, R.R., Rivas, F.J., Chávez, A.M., Dionysiou, D.D., 2020. Peroxymonosulfate/solar radiation process for the removal of aqueous microcontaminants. kinetic modeling, influence of variables and matrix constituents. J. Hazard. Mater. 400, 123118 https://doi.org/10.1016/j.jhazmat.2020.123118.

Solís, R.R., Rivas, F.J., Chávez, A.M., Dionysiou, D.D., 2019. Simulated solar photo-assisted decomposition of peroxymonosulfate. Radiation filtering and operational variables influence on the oxidation of aqueous bezafibrate. Water Res. 162, 383–393. https://doi.org/10.1016/j.watres.2019.06.063.

Tang, Y., Kang, J., Wang, M., Jin, C., Liu, J., Li, M., Li, S., Li, Z., 2021. Catalytic degradation of oxytetracycline via FeVO4 nanorods activating PMS and the insights into the performance and mechanism. J. Environ. Chem. Eng. 9, 105864 https://doi.org/10.1016/j.jece.2021.105864.

Travina, O.A., Ermakov, A.N., Kozlov, Y.N., Purmal, A.P., 2006. The absolute value of the rate constant of the liquid-phase reaction SO5−.+ Fe(II). Kinet. Catal. 47, 341–346. https://doi.org/10.1134/S0023158406030037.

Truong, T.K., Nguyen, T.Q., Phuong La, H.P., Le, H.V., Van Man, T., Cao, T.M., Van Pham, V., 2021. Insight into the degradation of p-nitrophenol by visible-light-induced activation of peroxymonosulfate over Ag/ZnO heterojunction. Chemosphere 268, 129291. https://doi.org/10.1016/j.chemosphere.2020.129291.

United Nations: Sustainable development goals, 2021 1258. ⟨https://www.un.org/sustainabledevelopment/water-and-sanitation/1259⟩.

United Nations: Water Policy Brief: Water Quality, 2011 1260 ⟨https://www.unwater.org/publications/un-water-policy-brief-water-quality⟩.

Wan, X., Qian, D., Ai, L., Jiang, J., 2020. Highly efficient peroxymonosulfate activation by surface oxidized nickel phosphide with dual active sites. Ind. Eng. Chem. Res. 59, 22040–22048. https://doi.org/10.1021/acs.iecr.0c04797.

Wang, C., Du, J., Liang, Z., Liang, J., Zhao, Z., Cui, F., Shi, W., 2022. High-efficiency oxidation of fluoroquinolones by the synergistic activation of peroxymonosulfate via vacuum ultraviolet and ferrous iron. J. Hazard. Mater. 422, 126884 https://doi.org/10.1016/j.jhazmat.2021.126884.

Wang, D., Luo, X., Yang, S., Xue, G., 2021. Tourmaline/perovskite composite material as heterogeneous catalysts for activation peroxymonosulfate to remove organic dye in water. J. Environ. Chem. Eng. 9, 105221 https://doi.org/10.1016/j.jece.2021.105221.

Wang, J., Wang, S., 2018. Activation of persulfate (PS) and peroxymonosulfate (PMS) and application for the degradation of emerging contaminants. Chem. Eng. J. 334, 1502–1517. https://doi.org/10.1016/j.cej.2017.11.059.

Wang, Z., Srivastava, V., Iftekhar, S., Ambat, I., Sillanpää, M., 2018. Fabrication of Sb2O3/PbO photocatalyst for the UV/PMS assisted degradation of carbamazepine from synthetic wastewater. Chem. Eng. J. 354, 663–671. https://doi.org/10.1016/j.cej.2018.08.068.

Wojnárovits, L., Tóth, T., Takács, E., 2020. Rate constants of carbonate radical anion reactions with molecules of environmental interest in aqueous solution: a review. Sci. Total Environ. 717, 137219 https://doi.org/10.1016/j.scitotenv.2020.137219.

Wu, S., Li, H., Li, X., He, H., Yang, C., 2018. Performances and mechanisms of efficient degradation of atrazine using peroxymonosulfate and ferrate as oxidants. Chem. Eng. J. 353, 533–541. https://doi.org/10.1016/j.cej.2018.06.133.

Wu, Y., Cai, T., Chen, X., Duan, X., Xu, G., Bu, L., Zhou, S., Shi, Z., 2021. Unveiling the interaction of epigallocatechin-3-gallate with peroxymonosulfate for degradation of bisphenol S: two-stage kinetics and identification of reactive species. Sep. Purif. Technol. 274, 119040 https://doi.org/10.1016/j.seppur.2021.119040.

Wu, Y., Yang, Y., Liu, Y., Zhang, L., Feng, L., 2019. Modelling study on the effects of chloride on the degradation of bezafibrate and carbamazepine in sulfate radical-based advanced oxidation processes: conversion of reactive radicals. Chem. Eng. J. 358, 1332–1341. https://doi.org/10.1016/j.cej.2018.10.125.

Xue, Y., Wang, Z., Bush, R., Yang, F., Yuan, R., Liu, J., Smith, N., Huang, M., Dharmarajan, R., Annamalai, P., 2021. Resistance of alkyl chloride on

chloramphenicol to oxidative degradation by sulfate radicals: kinetics and mechanism. Chem. Eng. J. 415, 129041 https://doi.org/10.1016/j.cej.2021.129041.
Yang, S., Wang, P., Yang, X., Shan, L., Zhang, W., Shao, X., Niu, R., 2010. Degradation efficiencies of azo dye Acid Orange 7 by the interaction of heat, UV and anions with common oxidants: persulfate, peroxymonosulfate and hydrogen peroxide. J. Hazard. Mater. 179, 552–558. https://doi.org/10.1016/j.jhazmat.2010.03.039.
Yu, Xiaolong, Li, M., Tang, S., Wei, Z., Yu, Y., Sun, J., Lu, G., Yin, H., 2021a. Photocatalysis of Tris-(2-chloroethyl) phosphate by ultraviolet driven peroxymonosulfate oxidation process: removal performance, energy evaluation and toxicity on bacterial metabolism network. Chem. Eng. J. 423, 130261 https://doi.org/10.1016/j.cej.2021.130261.
Yu, Xiaoping, Qin, W., Yuan, X., Sun, L., Pan, F., Xia, D., 2021. Synergistic mechanism and degradation kinetics for atenolol elimination via integrated UV/ozone/peroxymonosulfate process. J. Hazard. Mater. 407, 124393 https://doi.org/10.1016/j.jhazmat.2020.124393.
Yu, Xiaolong, Yu, Y., Wang, N., Li, M., Lu, G., Li, X., Niu, X., Sun, J., Yin, H., 2021b. Enhanced tris-(2-chloroisopropyl) phosphate degradation through ultraviolet driven peroxymonosulfate process: kinetics, mechanism, residual toxicity assessment of intermediates products by proteomics. Sci. Total Environ. 786, 147583 https://doi.org/10.1016/j.scitotenv.2021.147583.
Yu, Y., Tan, P., Huang, X., Tao, J., Liu, Y., Zeng, R.J., Chen, M., Zhou, S., 2020. Homogeneous activation of peroxymonosulfate using a low-dosage cross-bridged cyclam manganese(II) complex for organic pollutant degradation via a nonradical pathway. J. Hazard. Mater. 394, 122560 https://doi.org/10.1016/j.jhazmat.2020.122560.
Yuan, R., Wang, Z., Hu, Y., Wang, B., Gao, S., 2014. Probing the radical chemistry in UV/persulfate-based saline wastewater treatment: kinetics modeling and byproducts identification. Chemosphere 109, 106–112. https://doi.org/10.1016/j.chemosphere.2014.03.007.
Zalazar, C.S., Labas, M.D., Martín, C.A., Brandi, R.J., Cassano, A.E., 2004. Reactor scale-up in AOPs: from laboratory to commercial scale. Water Sci. Technol. 49, 13–18. https://doi.org/10.2166/wst.2004.0207.
Zhang, T., Márquez-Hernández, L.I., Arnold, R.G., Diefenthal, G., Sáez, A.E., 2019. Modeling the UV/H2O2 oxidation of phenolic compounds in a continuous-flow reactor with reflective walls. J. Environ. Chem. Eng. 7, 103150 https://doi.org/10.1016/j.jece.2019.103150.
Zhang, X., Chen, Z., Kang, J., Zhao, S., Wang, B., Yan, P., Deng, F., Shen, J., Chu, W., 2021. UV/ peroxymonosulfate process for degradation of chloral hydrate: pathway and the role of radicals. J. Hazard. Mater. 401, 123837 https://doi.org/10.1016/j.jhazmat.2020.123837.
Zhang, Z., Chuang, Y.-H., Szczuka, A., Ishida, K.P., Roback, S., Plumlee, M.H., Mitch, W. A., 2019. Pilot-scale evaluation of oxidant speciation, 1,4-dioxane degradation and disinfection byproduct formation during UV/hydrogen peroxide, UV/free chlorine and UV/chloramines advanced oxidation process treatment for potable reuse. Water Res. 164, 114939 https://doi.org/10.1016/j.watres.2019.114939.
Zhang, Z., Edwards, J.O., 1992. Chain lengths in the decomposition of peroxomonosulfate catalyzed by cobalt and vanadium. Rate law for catalysis by vanadium. Inorg. Chem. 31, 3514–3517. https://doi.org/10.1021/ic00043a007.
Zhao, J., Wei, H., Liu, P., Zhou, A., Lin, X., Zhai, J., 2021. Activation of peroxymonosulfate by metal–organic frameworks derived Co1+xFe2−xO4 for organic dyes degradation: a new insight into the synergy effect of Co and Fe. J. Environ. Chem. Eng. 9, 105412 https://doi.org/10.1016/j.jece.2021.105412.
Zhou, S., Yu, Y., Zhang, W., Meng, X., Luo, J., Deng, L., Shi, Z., Crittenden, J., 2018. Oxidation of microcystin-LR via activation of peroxymonosulfate using ascorbic acid: kinetic modeling and toxicity assessment. Environ. Sci. Technol. 52, 4305–4312. https://doi.org/10.1021/acs.est.7b06560.
Zhou, X., Jawad, A., Luo, M., Luo, C., Zhang, T., Wang, H., Wang, J., Wang, S., Chen, Zhulei, Chen, Zhuqi, 2021. Regulating activation pathway of Cu/persulfate through the incorporation of unreducible metal oxides: pivotal role of surface oxygen vacancies. Appl. Catal. B Environ. 286, 119914 https://doi.org/10.1016/j.apcatb.2021.119914.
Zhou, Y., Jiang, J., Gao, Y., Ma, J., Pang, S.-Y., Li, J., Lu, X.-T., Yuan, L.-P., 2015. Activation of peroxymonosulfate by benzoquinone: a novel nonradical oxidation process. Environ. Sci. Technol. 49, 12941–12950. https://doi.org/10.1021/acs.est.5b03595.
Zhou, Y., Jiang, J., Gao, Y., Pang, S.-Y., Yang, Yi, Ma, J., Gu, J., Li, J., Wang, Z., Wang, L.-H., Yuan, L.-P., Yang, Yue, 2017. Activation of peroxymonosulfate by phenols: important role of quinone intermediates and involvement of singlet oxygen. Water Res. 125, 209–218. https://doi.org/10.1016/j.watres.2017.08.049.